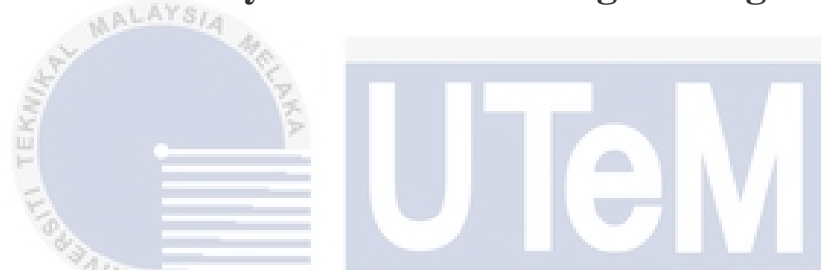




Faculty of Mechanical Engineering



**OPTIMIZATION OF SYNTHETIC JET ACTUATOR
LOCATION FOR AERODYNAMIC DRAG REDUCTION OF
BACKWARD-FACING STEP**

UNIVERSITI TEKNIKAL MALAYSIA MELAKA

Teo Yong Soon

Bachelor of Mechanical Engineering (Hons)

2018

**OPTIMIZATION OF SYNTHETIC JET ACTUATOR LOCATION FOR
AERODYNAMIC DRAG REDUCTION OF BAKWARD-FACING STEP**

TEO YONG SOON

**A thesis submitted
in fulfillment of the requirements for the Bachelor of Mechanical Engineering
(Hons)**



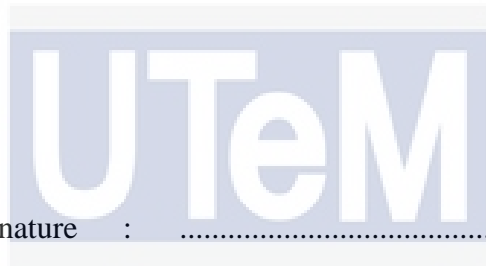
Faculty of Mechanical Engineering

UNIVERSITI TEKNIKAL MALAYSIA MELAKA

2018

DECLARATION

I declare that this thesis entitled “Optimization of Synthetic Jet Actuator Location for Aerodynamic Drag Reduction of Backward-facing Step” is the result of my own research except as cited in the references. The thesis has not been accepted for any degree and is not concurrently submitted in candidature of any other degree.



Signature :

Name :
اونيزر ستي تیکنیکل ملیسيا ملاک

Date :
UNIVERSITI TEKNIKAL MALAYSIA MELAKA

DEDICATION

To my beloved mother and father



APPROVAL

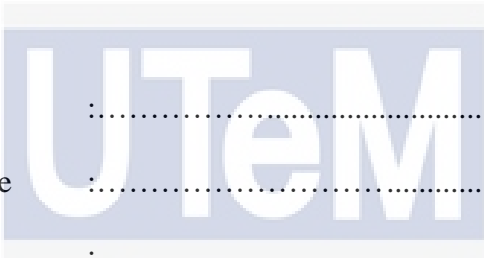
I hereby declare that I have read this dissertation/report and in my opinion this dissertation/report is sufficient in terms of scope and quality as a partial fulfillment of Bachelor of Mechanical Engineering (Hons).



Signature :

Supervisor Name :

Date :



اونيورسيتي تيكنيكل مليسيا ملاك

UNIVERSITI TEKNIKAL MALAYSIA MELAKA

ACKNOWLEDGEMENT

First, I would like to take this opportunity to express my grateful thanks to my supervisor Dr. Cheng See Yuan from Faculty of Mechanical Engineering University Teknikal Malaysia Melaka (UTeM) who had supervised, supported and guided me during this final year project. Besides, I appreciate the patient and generosity of Dr. Cheng See Yuan on teaching me about the ANSYS software.

After that, I would also like to express my grateful thanks to Msc. Jeffrey from Faculty of Mechanical Engineering University Teknikal Malaysia Melaka (UTeM) who had advised, helped and supported me during this final year project. I appreciate his patient on teaching me on the thesis writing.

Lastly, special thanks to all my beloved friends, girlfriend, mother, father and siblings for their moral and financial support in completing this final year project and my degree.

اونيورسيتي تيكنيكل مليسيا ملاك

UNIVERSITI TEKNIKAL MALAYSIA MELAKA

ABSTRACT

Active flow control is one of the aerodynamics flow control techniques that used to improve aerodynamics properties such as drag reduction, lift augmentation, noise mitigation and mixing enhancement by manipulating the boundary layer of the fluid flow. Synthetic jet actuator (SJA) is an active flow control device that used to manipulate the boundary layer by synthetic jet pulse producing by a vibrating membrane through a small orifice in order to improve the aerodynamics properties. The purpose of this study was to find an ideal location to locate the SJA in the backward-facing step and study the effect on the aerodynamic drag of the bluff body at different jet locations. The first simulation was performed on the SJA model in order to adopt an appropriate method to locate it in the backward-facing step. After that, a simulation was done on the backward-facing step without SJA (uncontrolled flow) in order to get the separation point for the simulation on the backward-facing step with SJA (controlled flow). A series of simulation was done on the controlled flow case in which the SJA located at separation point ($0.75h$), before separation point ($0.25h$), after separation point ($1.25h$) and SJA arrays at both separation and reattachment point ($0.75h$ and $2.0825h$). The study found out that the SJA arrays located at both separation point and reattachment point had the highest drag reduction of 26.05% while the single SJA located before separation point had the lowest drag reduction of only 0.84%. It was concluded that the best location to locate the SJA was at both separation and reattachment point.

ABSTRAK

Kawalan aliran aktif adalah salah satu kawalan aliran aerodinamik yang digunakan untuk menambah baik ciri-ciri aerodinamik seperti pengurangan seretan aerodinamik, peningkatan lif aerodinamik, pengurangan hingar dan peningkatan pencampuran dengan memanipulasi lapisan sempadan aliran bendalir. Aktuator jet sintetik (AJS) adalah satu alat kawalan aliran aerodinamik yang digunakan untuk memanipulasi lapisan sempadan dengan denyut jet sintetik yang dihasilkan oleh satu lapisan bergetaran melalui satu orifis yang kecil untuk menambah baik ciri-ciri aerodinamik. Tujuan kajian ini adalah untuk mencari lokasi yang ideal untuk melokasi AJS dalam domain aliran silang dan mengaji kesan pada seretan aerodinamik tubuh tebal dekat lokasi jet yang berbeza. Simulasi yang pertama adalah dilakukan pada modal AJS untuk mengadaptasi satu kaedah yang sesuai untuk melokasi AJS dalam domain aliran silang. Kemudian, simulasi telah dilakukan pada domain aliran silang tanpa AJS (aliran tidak terkawal) untuk mendapati titik pemisahan untuk simulasi pada domain aliran silang yang mempunyai AJS (aliran terkawal). Satu siri simulasi telah dilakukan pada kes aliran terkawal di mana AJS terletak pada titik pemisahan (0.75h), sebelum titik pemisahan (0.25h), selepas titik pemisahan (1.25h) dan susunan AJS yang terletak pada kedua-dua titik pemisahan dan titik pelekatan semula (0.75h and 2.0825h). Kajian ini mendapati bahawa susunan AJS yang terletak di kedua-dua titik pemisahan dan titik pelekatan semula mempunyai pengurangan seretan aerodinamik tertinggi sebanyak 26.05% manakala AJS tunggal yang terletak sebelum titik pemisahan mempunyai pengurangan seretan aerodinamik yang paling rendah iaitu hanya 0.84%. Kesimpulannya, lokasi terbaik untuk meletak AJS adalah pada kedua-dua titik pemisahan dan titik pelekatan semula.

TABLE OF CONTENTS

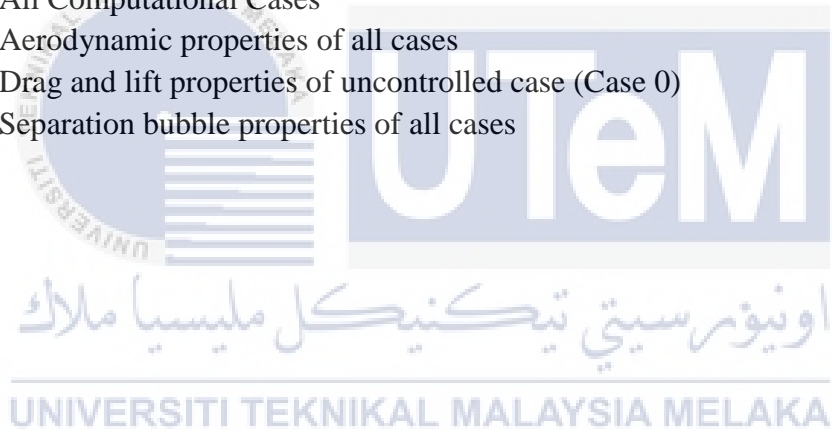
	PAGE
DECLARATION	
DEDICATION	
APPROVAL	
ACKNOWLEDGEMENTS	i
ABSTRACT	ii
ABSTRAK	iii
TABLE OF CONTENTS	iv
LIST OF TABLES	vi
LIST OF FIGURES	vii
LIST OF ABBREVIATIONS	x
LIST OF SYMBOLS	xi
CHAPTER	
1. INTRODUCTION	1
1.1 Background	1
1.2 Problem Statement	3
1.3 Objective	4
1.4 Scope of Project	4
2. LITERATURE REVIEW	5
2.1 Introduction	5
2.2 Synthetic Jet Actuator in Backward-facing Step Domain	7
2.3 Aerodynamics Drag	11
2.3.1 Boundary layer	11
2.3.2 Wake or flow separation	12
2.3.3 Drag reduction	13
2.4 Computational Study	14
2.4.1 Meshing	14
2.4.2 Turbulence model	15
2.4.3 Reynolds-Averaged Navier-Stokes (RANS) equation	16
2.4.4 Profile, contour and vector Plot	16
3. METHODOLOGY	18
3.1 Introduction	18
3.2 Synthetic Jet into Quiescent Flow	20
3.2.1 Geometry	21
3.2.2 Meshing	22
3.2.3 Fluent Setting	24
3.2.4 Validation and verification	25
3.2.4.1 Validation result	26

3.2.4.2 Sensitivity test on different domain size	26
3.2.4.3 Sensitivity test on different time step size	27
3.2.4.4 Sensitivity test on different boundary condition	29
3.3 Flow in Backward-facing Step	30
3.3.1 Geometry	30
3.3.2 Meshing	31
3.3.3 Fluent setting	32
3.3.4 Validation and verification	34
3.3.4.1 Validation result	34
3.3.4.2 Grid independency test	35
3.3.5 Result comparison	36
4. RESULT AND DISCUSSION	38
4.1 Synthetic Jet Actuator Location in the Backward-facing Step for All Cases	38
4.2 Effect of the Synthetic Jet Actuator Location in the Backward-facing Step on the Aerodynamic Drag	39
5. CONCLUSION AND RECOMMENDATIONS FOR FUTURE RESEARCH	46
REFERENCES	48



LIST OF TABLES

TABLES	TITLE	PAGE
2.1	Synthetic jet actuator locations (He Y. et al. 2001)	9
2.2	Cases with different forcing frequency and SJA location (Kotapati R. et al. 2006)	10
2.3	Location and size of separation bubble for different cases (Kotapati R. et al. 2006)	11
3.1	Drag coefficient of different mesh cells	35
4.1	All Computational Cases	38
4.2	Aerodynamic properties of all cases	40
4.3	Drag and lift properties of uncontrolled case (Case 0)	42
4.4	Separation bubble properties of all cases	42



LIST OF FIGURES

FIGURE	TITLE	PAGE
2.1	Schematic of general Synthetic Jet Actuator (Zhou et al. 2015)	6
2.2	Schematic of Synthetic Jet Actuators	6
2.2 (a)	Single diaphragm (Xiong et al. 2010)	6
2.2 (b)	Double diaphragm (Kurowski et al. 2015)	6
2.3	Synthetic jet formation parameters (Murugan et al. 2016)	7
2.4	Lift coefficient increment at different jet locations (Zhao G. et al 2014)	9
2.5	Mean streamwise velocity field and separation bubbles streamlines (Dandois J. 2006)	10
2.5 (a)	Uncontrolled flow (Dandois J. 2006)	10
2.5 (b)	Low frequency controlled flow (Dandois J. 2006)	10
2.5 (c)	High frequency controlled flow (Dandois J. 2006)	10
2.6	Types of boundary layers (Fox R.W. et al. 2010)	12
2.7	Flow separation occur inside a wide angle diffuser (Cengel Y.A. et al 2006)	13
2.8	Classification of the flow control techniques (El-Alti M. et al. 2012)	14
2.9	Structured and unstructured mesh (Cengel Y.A. et al 2006)	15
2.10	Types of plot (Cengel Y.A. et al 2006)	17
2.10 (a)	Profile plot (Cengel Y.A. et al 2006)	17
2.10 (b)	Vector plot (Cengel Y.A. et al 2006)	17
2.10 (c)	Contour plot (Cengel Y.A. et al 2006)	17
3.1	Simulation Flow Chart	19
3.2	Modelling and Simulation phases and V&V roles (Schlesinger, S. et al. 1979)	20
3.3 (a)	Verification Process (Oberkampf, W.L. et al. 2002)	20
3.3 (b)	Validation Process (Oberkampf, W.L. et al. 2002)	20
3.4	Dimension of synthetic jet actuator model	21
3.5	Geometry of synthetic jet actuator model	22
3.6	Mesh of synthetic jet actuator model	23
3.7	Boundary condition of the fluid domain (left) and synthetic jet actuator (right)	23
3.8	User-defined function of the cavity wall motion	25

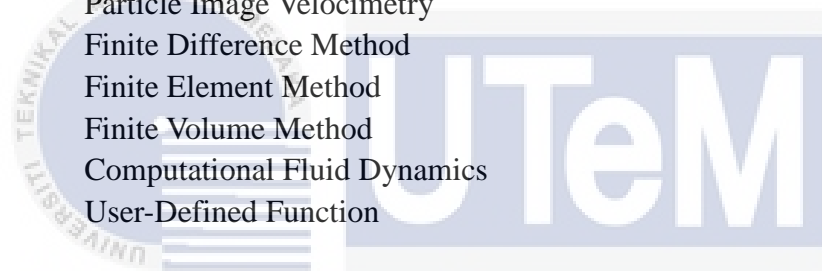
3.9	Comparison of the time-averaged velocity distributions between experiment results and synthetic jet actuator model at $z = 9.8\text{mm}$	26
3.10	Graph of average z-velocity versus flow time at orifice exit for domain size $161D_o$, $181D_o$ and $201D_o$	27
3.11	Graph of average z-velocity versus flow time at orifice exit for time step size 8.33×10^{-6} (120 time step per cycle), 5.56×10^{-6} (180 time step per cycle) and 4.17×10^{-6} (240 time step per cycle)	28
3.12	Graph of average z-velocity versus flow time at orifice exit for periodic boundary condition and symmetry boundary condition	29
3.13	Graph of z-velocity versus x-axis position at orifice exit for periodic boundary condition and symmetry boundary condition	30
3.14	Dimension of backward-facing step model	31
3.15	Geometry of backward-facing step	31
3.16	Mesh of backward-facing step	32
3.17	Boundary condition of the backward-facing step	32
3.18	User-defined function of the synthetic jet velocity profile	33
3.19	Time-averaged streamwise velocity $x/h + u/U_\infty$ (solid line: RANS, dotted line: DNS)	34
3.20	Graph of average drag coefficient at slope versus number of mesh cells	36
3.21	Graph of drag coefficient versus flow time at the slope for four different mesh cells	36
4.1	Streamline profile of the uncontrolled flow case (Case 0) and the location of the separation point	39
4.2	Streamline profile of the controlled flow case (Case 1) and the location of the reattachment point	39
4.3	Graph of drag coefficient versus flow time at the slope for all cases	40
4.4	Graph of lift coefficient versus flow time at the slope for all cases	41
4.5 (a)	Pressure contour of all cases after blowing stroke at $t = 4.5 \times 10^{-3}\text{s}$ – Case 0	43
4.5 (b)	Pressure contour of all cases after blowing stroke at $t = 4.5 \times 10^{-3}\text{s}$ – Case 1	43
4.5 (c)	Pressure contour of all cases after blowing stroke at $t = 4.5 \times 10^{-3}\text{s}$ – Case 2	43
4.5 (d)	Pressure contour of all cases after blowing stroke at $t = 4.5 \times 10^{-3}\text{s}$ – Case 3	43
4.5 (e)	Pressure contour of all cases after blowing stroke at $t = 4.5 \times 10^{-3}\text{s}$ – Case 4	43
4.6 (a)	Streamline profile of all cases – Case 0	44
4.6 (b)	Streamline profile of all cases – Case 1	44
4.6 (c)	Streamline profile of all cases – Case 2	44
4.6 (d)	Streamline profile of all cases – Case 3	44
4.6 (e)	Streamline profile of all cases – Case 4	44

4.7 (a)	Vorticity contour of all cases – Case 0	45
4.7 (b)	Vorticity contour of all cases – Case 1	45
4.7 (c)	Vorticity contour of all cases – Case 2	45
4.7 (d)	Vorticity contour of all cases – Case 3	45
4.7 (e)	Vorticity contour of all cases – Case 4	45



LIST OF ABBREVIATIONS

AFC	Active Flow Control
SJA	Synthetic Jet Actuator
ZNMF	Zero-Net Mass-Flux
RANS	Reynolds-Average Navier-Stokes
URANS	Unsteady Reynolds-Average Navier-Stokes
SST	Shear Stress Transport
AOA	Angle of Attack
PIV	Particle Image Velocimetry
FDM	Finite Difference Method
FEM	Finite Element Method
FVM	Finite Volume Method
CFD	Computational Fluid Dynamics
UDF	User-Defined Function



اونيورسيتي تيكنيكل مليسيا ملاك

UNIVERSITI TEKNIKAL MALAYSIA MELAKA

LIST OF SYMBOLS

Ma	Mach Number
Re	Reynolds Number
c	Chord Length
α	Angle of Attack
f_J	Forcing Frequency
f_{SEP}	Separation Bubble Frequency
f_{SL}	Shear Layer Frequency
x_{SEP}	Separation Location
L_{SEP}	Separation Bubble Length
ΔL_{SEP}	Separation Bubble Length Increment
H_{SEP}	Separation Bubble Height
ρ	Density
v	Velocity
F_D	Drag Force
A	Frontal Area
C_D	Drag Coefficient
ΔC_D	Drag Coefficient Increment
C_L	Lift Coefficient
ΔC_L	Lift Coefficient Increment
x_i	Location in x-direction
x_j	Location in y-direction
x_s	Separation Point Location in x-direction
x_r	Reattachment Point Location in x-direction
F_i	Force in x-direction
F_{DP}	Pressure Drag Force
F_{DV}	Viscous Drag Force
F_{LP}	Pressure Lift Force
F_{LV}	Viscous Lift Force
v_i	Velocity in x-direction
v_j	Velocity in y-direction
v_{SJA}	Synthetic Jet Velocity
v_{max}	Maximum Jet Velocity
μ	Kinematics Viscosity
h	Step height

$z_{cavity\ wall}$	Cavity wall Location in z-direction
A	Amplitude
f	Frequency
t	Time
D_o	Orifice Width
N	Number of Time Step



CHAPTER 1

INTRODUCTION

1.1 Background

Aerodynamics flow control technique has been widely researched and developed in order to improve the aerodynamics properties in several sectors. Among the aerodynamics flow control techniques, active flow control (AFC) is one of the types of aerodynamics flow control techniques which are usually used in manipulating the boundary layer to improve aerodynamics properties in various applications. Those applications consist of drag reduction, lift augmentation, noise mitigation and mixing enhancement. In the active flow control device, momentum or energy is always added to the flow in a regulated manner in order to help in the control of the fluid flow. In the past decades, plenty of researches showed that active flow controls technique has provided solution for the problem faced by the aerodynamic transport applications and electronic cooling applications. Active flow control technique device such as synthetic jet actuator had helped to reduce aerodynamics drag of the vehicle for about 15.83% in suction and 14.38% in blowing (Harinaldi et al. 2011). Besides that, an appropriate combination of jet arrays in active flow control technique had increase both lift coefficient and drag coefficient of the passenger van by 100% and 26.5% respectively (Zhao G. et al. 2014). For active flow control devices in electronic cooling applications, larger hydraulic diameter and smaller

aspect ratio orifices had a best result in the heat transfer (Lee et al. 2016).

Synthetic jet actuator (SJA), also can be called as Zero-Net Mass-Flux (ZNMFL) actuator is a device that uses in active flow control technique by using synthetic jet produces by a vibrating membrane through an orifice. In fluid dynamics, synthetic jet flow is a type of jet flow which is usually created by an actuator with one or two vibrating diaphragm where the stream of one fluid mixes with the surrounding medium (Kurowski et al. 2015). In flow control applications, SJA is use to create a formation of vortex ring pair in order to impart momentum on the boundary layer of the flow. The performance of the synthetic jet usually depends on either the parameter of the actuator or the properties of the fluid. The various parameters of the actuator that influence the performance of the synthetic jet are normally diaphragm vibration properties, cavity dimensions, cavity shape, orifice dimensions and orifice shape. According to the research of the past decades, the performance of the synthetic jet is based on the velocity of the synthetic jet, vorticity and pressure contours produce by the synthetic jet. In active flow control, the cavity shapes of the actuator did not have large impact on the performance of the synthetic jet (Feero et al. 2015). Besides that, for different actuator's parameters, different excitation frequency of the diaphragm will have difference performance (Lv Yuan-wei et al. 2014). This study shows that the performance of the synthetic jet can be achieves by finding the optimal design for each parameter and the suitable excitation frequency for the actuator. Moreover, by using double vibrating diaphragm and higher vibrating amplitude, the results showed massive increasing in the jet velocity with the same membrane and cavity resonant frequency (Kurowski et al. 2015).

A bluff body in fluid mechanics can be defined as a body that the drag force experience by the body is dominant by pressure drag due to the shape of the body which has separated flow over a substantial part of its surface. A bluff body flow involve in interaction of 3 shear layers which will influence the aerodynamics properties which are boundary layer, separating free shear layer and the wake. In the aerodynamics of bluff body, the aerodynamics properties improvements that will usually be consider are the aerodynamic drag reduction, lift enhancement, vibration and noise reduction. In order to achieve those improvements, it is important to control the wake and the dynamics of vortex formations which acts as the source of fluid forces of the bluff body (Efstathios Konstantinidis et al. 2016). Those controls can be done by using passive or active flow control techniques.

1.2 Problem Statement

Aerodynamic properties such as aerodynamic drags of the bluff body such as building and transportation acts as an importance factors in reducing power consumption and higher height construction probability. Therefore, the active flow control device such as synthetic jet actuator was introduced to help in the reducing the aerodynamic drag of the bluff body. In order to achieve a better drag reduction of the bluff body, it is necessary to study the ideal location to locate the synthetic jet actuator.

1.3 Objective

The objectives of this final year project are as follows:

1. To find an optimal design on the location of the synthetic jet actuator in the backward-facing step.
2. To study the effect of the synthetic jet actuator position in the backward-facing step on the aerodynamic drag of the bluff body.

1.4 Scope of Project

The scopes of this final year project are:

1. Only the effect of the synthetic jet actuator's location on the aerodynamic drag in the backward-facing step will be study in this report.
2. Turbulence flow will be simulated inside the backward-facing step.
3. The analysis of the performance of the synthetic jet and aerodynamic drag of the bluff body will be conduct by using simulation by ANSYS-Computational Fluid Dynamic (CFD) software in this report.

CHAPTER 2

LITERATURE REVIEW

2.1 Introduction

Active flow devices have a high potential to use in jet's thrust vectoring, mixing enhancement, heat transfer, drag reduction and separation in flow regimes reduction (Saambavi et al. 2014). A general synthetic jet actuator (SJA) (Fig. 2.1) is one of the types of active flow control device that contains of a cavity with an oscillating diaphragm and a small orifice (Zhou et al. 2010). There were also some different kinds of orientation of diaphragm of the synthetic jet actuator such as double diaphragm parallel to the orifice exit (Fig. 2.2(b)) (Kurowski et al. 2015) and single diaphragm parallel to the orifice exit (Fig. 2.2(a)) (Xiong et al. 2013). The generation of the synthetic jet was caused by the volume change in the cavity due to the fluctuation of the oscillating diaphragm. During the suction stroke, the diaphragm of the SJA will move downwards and causes the fluid from the surrounding medium to enter the cavity. During blowing stroke, the diaphragm of the SJA will move upwards, causing the fluid inside the cavity push out from the cavity through the small orifice in the form of a jet. When the fluid pass through the orifice during both suction and blowing stroke, a shear layer will form which causing a rolling vortex ring formed at the orifice (Zhou et al. 2010). The formation of synthetic jet is governed by some of the parameters such as actuator diaphragm parameters, actuator geometry parameters

and the fluid domain parameters (Fig. 2.3). Besides than the actuator and fluid parameters, the synthetic jet can also be characterized by the non-dimensional parameters such as Reynolds number, Strouhal number, Stokes number and stroke ratio (Murugan et al. 2016).

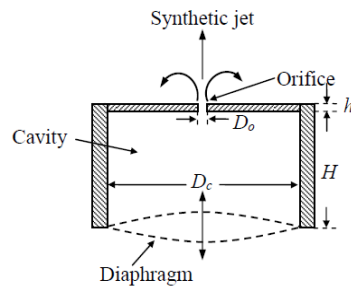
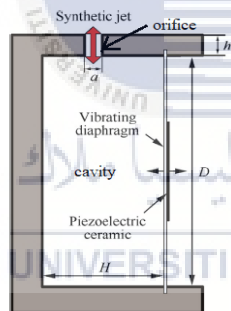


Figure 2.1: Schematic of general Synthetic Jet Actuator (Source: Zhou et al. 2015)

(a)



(b)

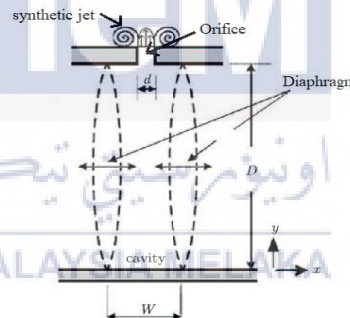


Figure 2.2: Schematic of Synthetic Jet Actuators with (a) single diaphragm (Source: Xiong et al. 2010) and (b) double diaphragm (Source: Kurowski et al. 2015).

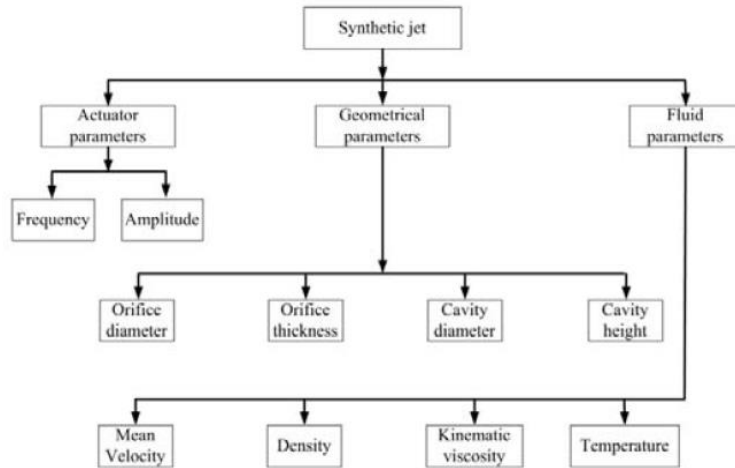


Figure 2.3: Synthetic jet formation parameters (Source: Murugan et al. 2016)

2.2 Synthetic Jet Actuator in Backward-facing Step

Many recent studies and researches had conducted the effect of the different in the location of the synthetic jet actuator in the backward-facing step. In the study done on the effect of the synthetic jet control on the separation, the simulation conducted by using unsteady coupled turbulence $k-\omega$ SST Reynolds-Averaged Navier-Stokes (URANS) equations with subsonic stream flow of $Ma = 0.4$ on the OA213 rotor airfoil. The oscillating diaphragm motion of the SJA on the airfoil was replaced with a sinusoidal velocity boundary condition with orifice width of $1\%c$, oscillatory frequency and momentum of 1.0 and 0.0007 respectively. In the simulation for the analysis of jet locations at $5\%c$, $15\%c$, $30\%c$, $45\%c$ and $60\%c$, the results showed that at small AOA and high AOA, placing the SJA at $15\%c$ and $5\%c$ has the best effect on lift increment respectively. Besides, they also study the combination of jet array on the effect of the lift increment and the results showed that the jet arrays have a better effect on the lift increment compared to single jet where the lift increment and drag reduction could be

improved by nearly 100% and 26.5% (Zhao G. et al. 2014). Besides than that, an experimental study conducted on the investigation of the SJA location at the leading and trailing edge of the airfoil inside a smoke tunnel. In the experiment results, it showed that at lower stream velocity, $v = 10\text{m/s}$ and $Re = 180000$, the combination of SJA array at trailing and leading edge had the best effect on the lift increment and for higher stream velocity, $v = 25\text{m/s}$ and $Re = 440000$, the SJA location at trailing edge had the best lift increment at AOA of $5^\circ < \alpha < 20^\circ$ while the leading edge had the best lift increment at AOA of $18^\circ < \alpha < 23^\circ$ but combination of SJA array does not had any significant effect on the lift increment (Krishnappa S. et al 2016). Other than that, another experiment study on the effect of the SJA location at 15%c and 40%c with different jet and phase angles at the thick airfoil by using PIV, the results showed that at the SJA location near to the leading edge had significant effects in delaying the stall but the SJA array had a better flow control performances than single SJA. Besides, a 180° phase difference of SJA array at AOA just reaching and larger than the stall AOA had significant lift increment and flow separation prevention (Zhao G. et al. 2016). Moreover, a computational study on the effect of different SJA location on stall control of airfoil using two-dimensional incompressible SST turbulence RANS model was conducted, the simulation was done by placing the SJA at five different locations (Table. 2.1) along the airfoil. The simulation results showed that the location of the SJA near the point of separation flow occurs had the best performance (He Y. et al. 2001).

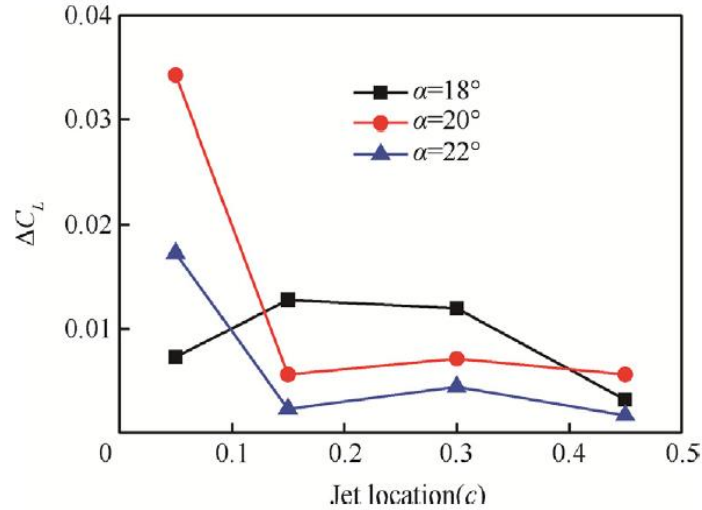


Figure 2.4: Lift coefficient increment at different jet locations (Source: Zhao G. et al., 2014)

Table 2.1: Synthetic jet actuator locations (He Y. et al. 2001)

Name of Jet Slot	x/c (%)
A	0.36 – 0.7
B	0.7 – 0.97
C	0.97 – 1.29
D	1.29 – 1.61
E	1.61 – 1.94

Besides than the location of the synthetic jet, a numerical study was done on the effect of the SJA on the separation length with two different SJA forcing frequencies of 720Hz (low frequency) and 5800Hz (high frequency), the simulation results showed that the low frequency, the separation length was reduced by 54% and increase by 43% for high forcing frequency compared to uncontrolled flow which can be shown in Figure 2.5 (Dandois J. 2006). Another numerical study on the effect of the SJA forcing frequency on the separation bubble was conducted, the simulation was done on seven different forcing frequency cases (Table 2.2). The final simulations results showed that the SJA with the

forcing frequency, f_J less than the separation bubble frequency, f_{SEP} has better effect on delaying and reduced the separation point and separation bubble size respectively (Table. 2.3) (Kotapati R. et al. 2006).

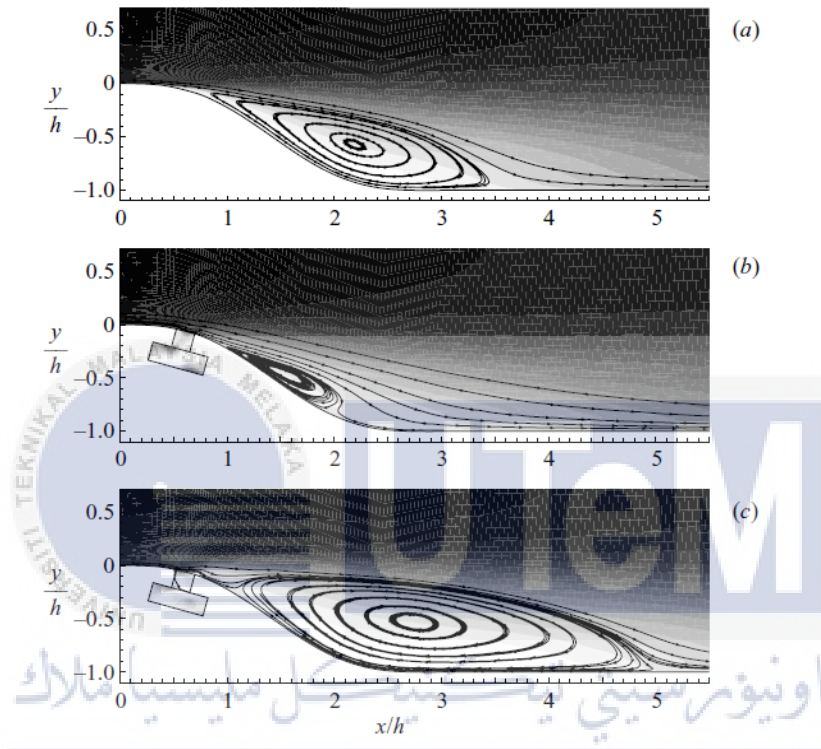


Figure 2.5: Mean streamwise velocity field and separation bubbles streamlines: (a) uncontrolled flow, (b) low frequency controlled flow and (c) high frequency controlled flow (Source: Dandois J. 2006)

Table 2.2: Cases with different forcing frequency and SJA location (Kotapati R. et al. 2006)

Case	Forcing Frequency, f_J	SJA location, x_J/c
1	No f_J	0.2
2	$f_{SEP}/2$	0.2
3	f_{SEP}	0.2
4	$f_{SL} = 2 f_{SEP}$	0.2
5	$2f_{SL}$	0.2
6	$2f_{SL} \pm f_{SEP}$	0.2
7	f_{SEP}	0.4

Table 2.3: Location and size of separation bubble for different cases (Kotapati R. et al. 2006)

<i>Case</i>	x_{SEP}/c	L_{SEP}/c	H_{SEP}/c
1	0.239	0.331	0.030
2	-	-	-
3	-	-	-
4	0.264	0.156	0.005
5	0.236	0.337	0.031
6	0.245	0.213	0.014
7	0.239	0.293	0.024

2.3 Aerodynamics Drag

In fluid mechanics, aerodynamic drag is the force exerted on the body by the flowing fluid in the direction of the flow. The drag coefficient is a function of density ρ of fluid, fluid velocity v , drag force F_D and the frontal area A of the body (Cengel Y.A. et al. 2006).

$$\text{drag coefficient, } C_D = \frac{2F_D}{\rho Av^2} \quad (2.1)$$

Besides, pressure drag is one type of drag that the resolved components of forces of the flowing fluid are acting to the normal of the body or surface (Houghton E.L. et al. 2012).

2.3.1 Boundary layer

Boundary layer is the region within the fluid flow which the viscous effect of the fluid is significant. The thickness of the boundary layer highly depends on the Reynolds number in which a high Reynolds number indicate a thicker boundary layer and vice versa (Cengel Y.A. et al. 2006). The flow of the boundary layer can be categorized into laminar, transition

and turbulent (Fig. 2.6). The boundary layer transition is affected by several factors such as flow pressure gradient, body surface roughness, heat transfer, forces acting on the body and the disturbance of the freestreams (Fox R.W. et al. 2010).

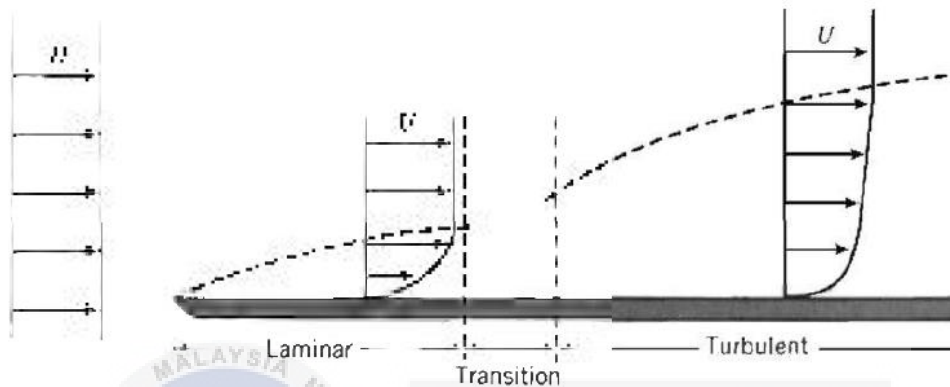


Figure 2.6: Types of boundary layers (Source: Fox R.W. et al. 2010)

2.3.2 Wake or flow separation

The flow separation is a phenomenon where the boundary layer of the fluid is seen to separate off the wall of the body due to adverse pressure gradient. The fluid particles in the boundary layer that insufficient of momentum are forced to change the flow direction which causing this “separation” phenomenon to occur. The magnitude of the pressure drag force depends on the size of the separation region. Besides, the location of the flow separation depends on Reynolds number, surface roughness and the level of the free stream fluctuations. Wake is the region where the velocity of the fluid is decrease due to flow separation (Cengel Y.A. et al. 2006), (Anderson et al. 2011).

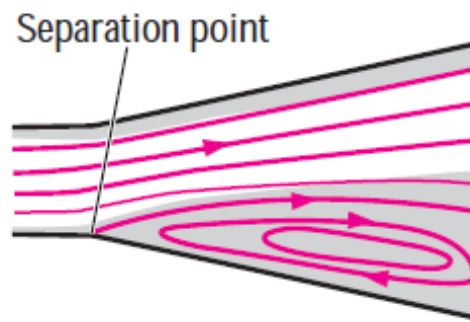


Figure 2.7: Flow separation occur inside a wide angle diffuser (Source: Cengel Y.A. et al. 2006)

2.3.3 Drag reduction

There are two techniques that used to reduce the drag which are active flow control and passive flow control. The passive flow control is a technique used to control the flow or generate desire flow behaviour by using geometry modification or addition. For an example, the vortex generator is a type of passive flow devices that widely used on the airplane to control the delay the flow separation by generating vortex to disturb the boundary layer (El-Alti M. et al. 2012). Active flow control is a technique that interacts dynamically with the fluid by imparts energy on the fluid flow by the use of devices. A synthetic jet actuator is an active flow control device that imparts the energy to the fluid flow by suction and blowing process (Mello H.C. et al. 2007).

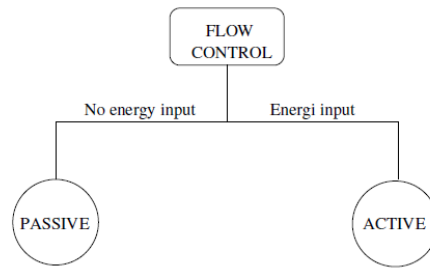


Figure 2.8: Classification of the flow control techniques (Source: El-Alti M. et al. 2012)

2.4 Computational Study

It can be general seen that the computational tools are used to simulate the flow control in which the computational fluid dynamics had provided an understanding of the flow control physics (Montazer E. et al. 2016).

2.4.1 Meshing

In computational fluid dynamics analysis, numerical method is use to find the behaviour and effect of fluid flow by using a set of differential equations. This numerical method can be categorized into 3 types of discretization methods which are finite difference method, finite element method and finite volume method. Finite difference method (FDM) is a method which uses to solve differential equations on the uniform mesh grids by approximate the derivatives of differential equation by using Taylor's approximation theory. Finite element method (FEM) also can be refer as finite element analysis (FEA) is usually use to analyse the common problems in structural analysis. It uses subdivision of larger problem into smaller finite elements to solve a large problem and uses variation method to approximate solution in the analysis. Finite volume method (FVM)

is the technique that commonly uses in the mesh generation in computational fluid dynamics (CFD) in ANSYS fluent. In FVM, the domain was first divides into smaller control volumes or cells where the variables of interest located at the centroid. Then, by using interpolation method, the differential equations were integrated over each control volume into discretized equations which express the conservation principle for each quantity such as mass, momentum, energy and species inside the elements (Laha D. et al. 2015).

The mesh generation contains of unstructured mesh and structured mesh where unstructured mesh is made up by tetrahedral or combination of hexagonal and tetrahedral mesh cell while the structured mesh is made up by either tetrahedral mesh cell or hexagonal mesh cell (Langtry R. et al. 2006).

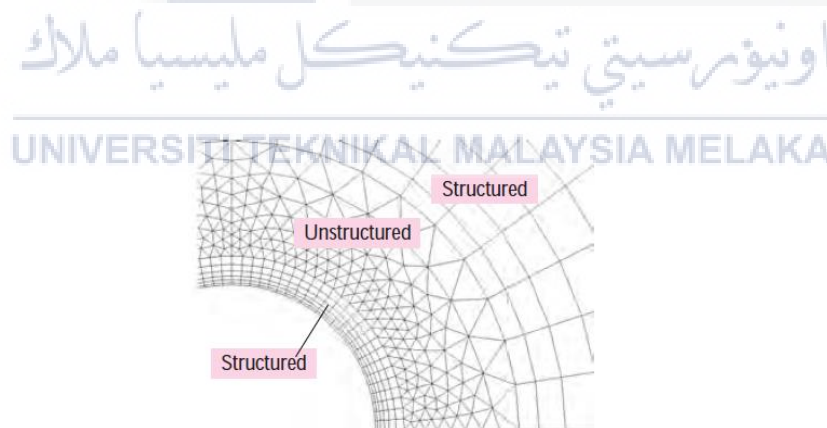


Figure 2.9: Structured and unstructured mesh (Source: Cengel Y.A. et al. 2006)

2.4.2 Turbulence model

The selection of the turbulence model is very importance in the simulation of computational fluid dynamics as it may affect the results of the simulation (Council et al.

2012). Spalart-Allmaras is one of the one equation turbulence models that mainly developed for aerodynamics flow. It is normally a transport equation for eddy viscosity in aerodynamics fluid flow (Javaherci T. et al. 2010).

2.4.3 Reynolds-Averaged Navier-Stokes (RANS) equation

The Reynolds-Averaged Navier-Stokes equation is the equation used for the isotropic, Newtonian fluid which can be defined by Eq. (2.2)

$$\rho \frac{Dv_i}{Dt} = F_i - \frac{\partial p}{\partial x_i} + \frac{\partial}{\partial x_j} \left[\mu \frac{\partial v_i}{\partial x_j} + \frac{\partial v_j}{\partial x_i} \right] - \frac{\partial}{\partial x_i} \left(\frac{2}{3} \mu \frac{\partial v_j}{\partial x_j} \right) \quad (2.2)$$

which named after Claude-Louis Navier and George Gabriel Stokes. The URANS computation is enough for the simulation of the synthetic jet motion besides than using LES and DNS in the engineering point of view (Dandois J. et al. 2006).

UNIVERSITI TEKNIKAL MALAYSIA MELAKA

2.4.4 Profile, contour and vector plot

In simulation results, profile plot is the simplest plot to visualise the value of the scalar properties along the interest direction in the flow field. The example of the scalar properties are pressure, temperature, density, velocity and so on. If the velocity profile plot is plotted with arrows, the velocity profile plot will becomes the velocity vector plot. Vector plot is the combinations of vector arrows that shows the direction and magnitude of the vector property at a particular time of the fluid flow. Vector plot is very useful in showing the flow pattern for both experiment and computational fluid flow. The magnitude

of the vector property depends on the size and colour of the arrow. Besides that, the contour plot was used to show curves of scalar or vector property of a particular time by using a set of colours (Cengel Y.A. et al 2006).

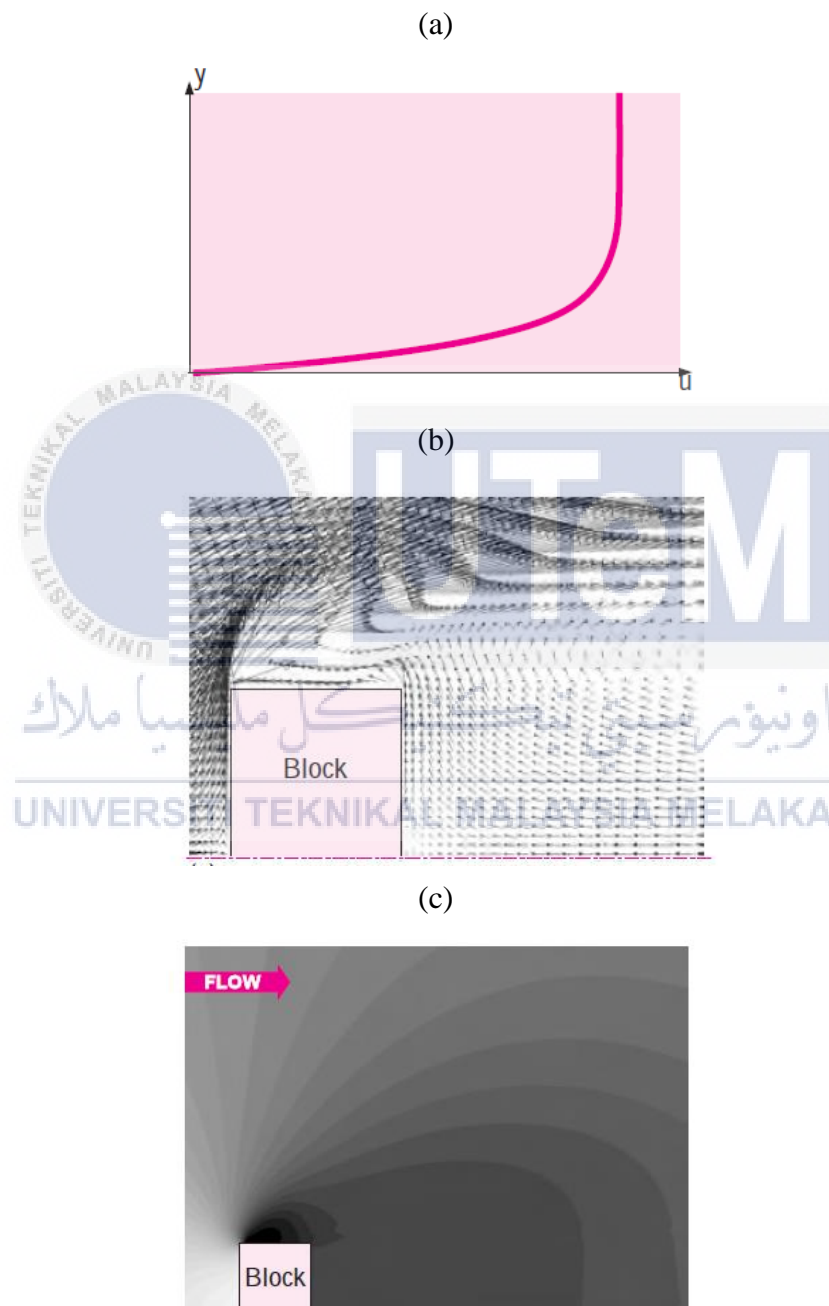


Figure 2.10: Types of plot (a) Profile plot, (b) Vector plot, and (c) Contour plot (Source: Cengel Y.A. et al. 2006)

CHAPTER 3

METHODOLOGY

3.1 Introduction

This final year project will mainly focused on the study of the effect of synthetic jet produced by different actuator's parameter on the aerodynamic flow properties of the bluff body through computational fluid dynamics (CFD) methods. This chapter covered every single details of the methodology methods used in order to achieve the objectives that had been set in this project by using a set of simulation procedures that will be conducted in the appropriate flow manner which shown in Figure 3.1. The project started with selecting the appropriate models from the previous research paper that was suitable for this project's title which the models chose were the synthetic jet actuator model developed by Okada K. et al. (2010) and the backward-facing step model developed by Dandois J. et al. (2006).

Then, the geometry and meshing of the both models were created. After the creation of the geometry and meshing, the validation and verification of both models were conducted. Verification and validation (V&V) is a process that used to determine the correctness of the implemented conceptual model and the accuracy of the simulation to the physical reality respectively which shown in Figure 3.2 and Figure 3.3. In this project, the validation process of the synthetic jet actuator was done by compared the time-averaged velocity distribution graph from Okada's paper while the verification was done on the sensitivity

test of different domain size, time step size and boundary condition. For backward-facing step, the validation was done on the comparison of the time-averaged streamwise velocity profile from Dandois's paper and the verification was done on the grid independency test for different mesh elements.

After that, the fluid flow in backward-facing step domain without synthetic jet (uncontrolled flow case) was simulated using the validated fluent setting in order to find the location of the separation point. Then, four different synthetic jet locations cases were chose and the simulations were done by using ANSYS software. Lastly, the results attained from the simulation were compared and the conclusion was made.

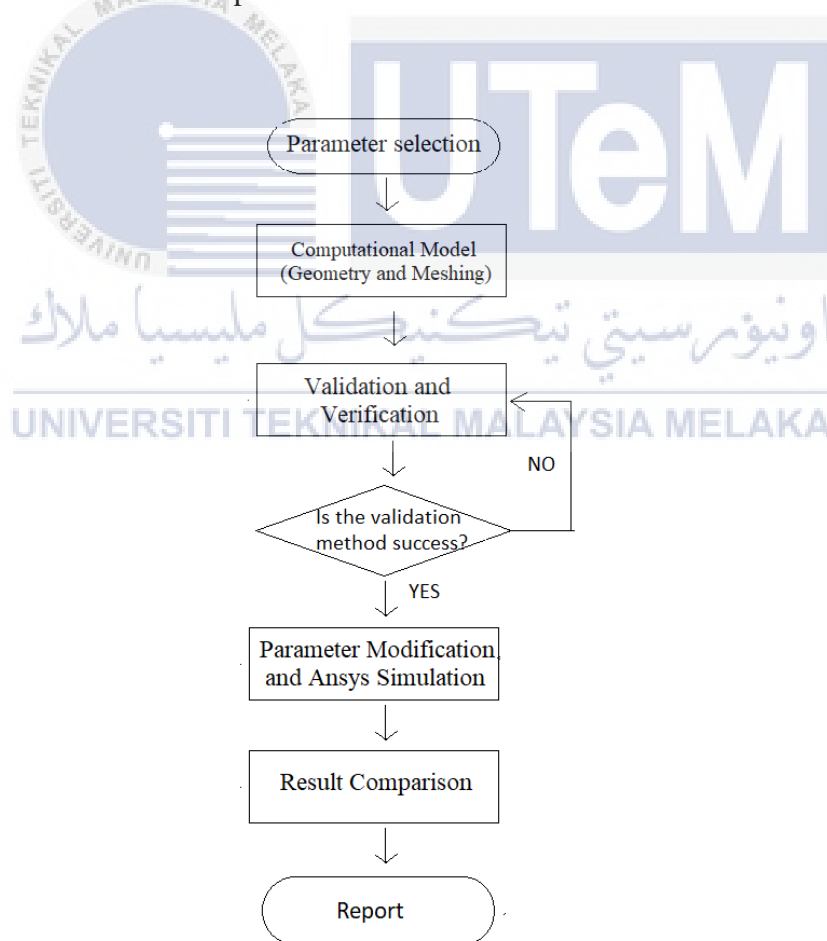


Figure 3.1: Simulation Flow Chart

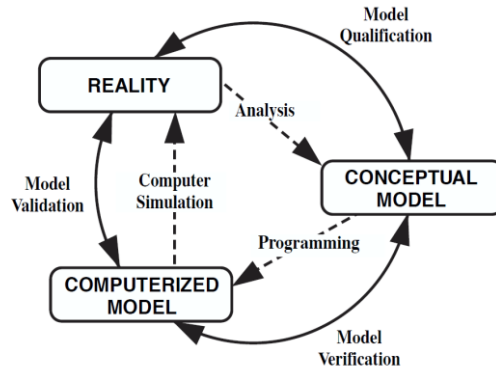


Figure 3.2: Modelling and Simulation phases and V&V roles
(Source: Schlesinger, S. et al. 1979)

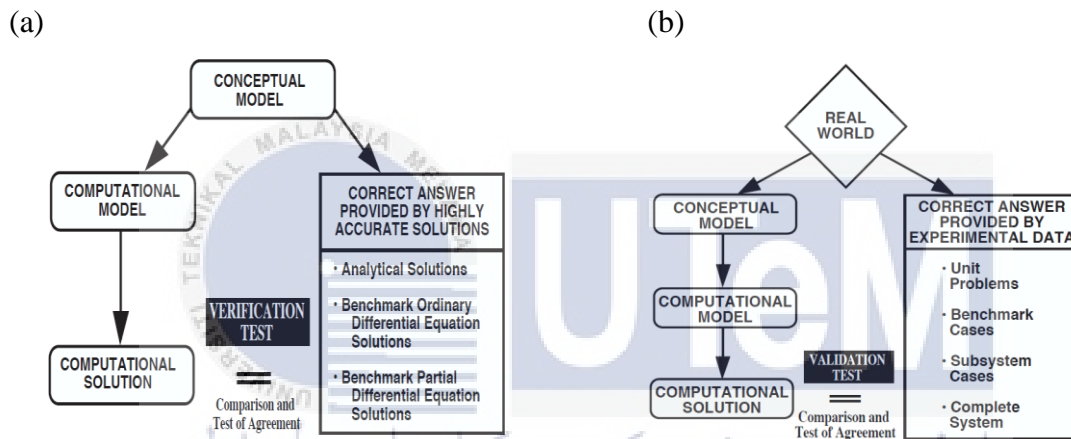


Figure 3.3: (a) Verification Process (b) Validation Process
(Source: Oberkamp, W.L. et al. 2002)

3.2 Synthetic Jet into Quiescent Flow

The synthetic jet into quiescent flow was studied by created a synthetic jet actuator model with a vibrating diaphragm in which the motion of the vibrating diaphragm was generated by using user-defined function. In this project, the purpose of creating this model was to study the properties of the synthetic jet itself in order to found out the idea to locate the device in the backward-facing step.

3.2.1 Geometry

The dimension of the synthetic jet actuator model was shown in the Figure 3.4. The computational fluid domain of the synthetic jet actuator has a dimension of $161D_o \times 500D_o \times 8D_o$ where the orifice width, $D_o = 1\text{mm}$ while the synthetic jet actuator has the dimension of $15\text{mm} \times 10\text{mm} \times 8\text{mm}$. The geometry of the synthetic jet actuator had been created as shown in Figure 3.5. The purpose of the slicing of the synthetic jet actuator's geometry into several sections near the orifice of the actuator in the DesignModeler was to create finer mesh at the orifice exit area and coarser mesh at the others.

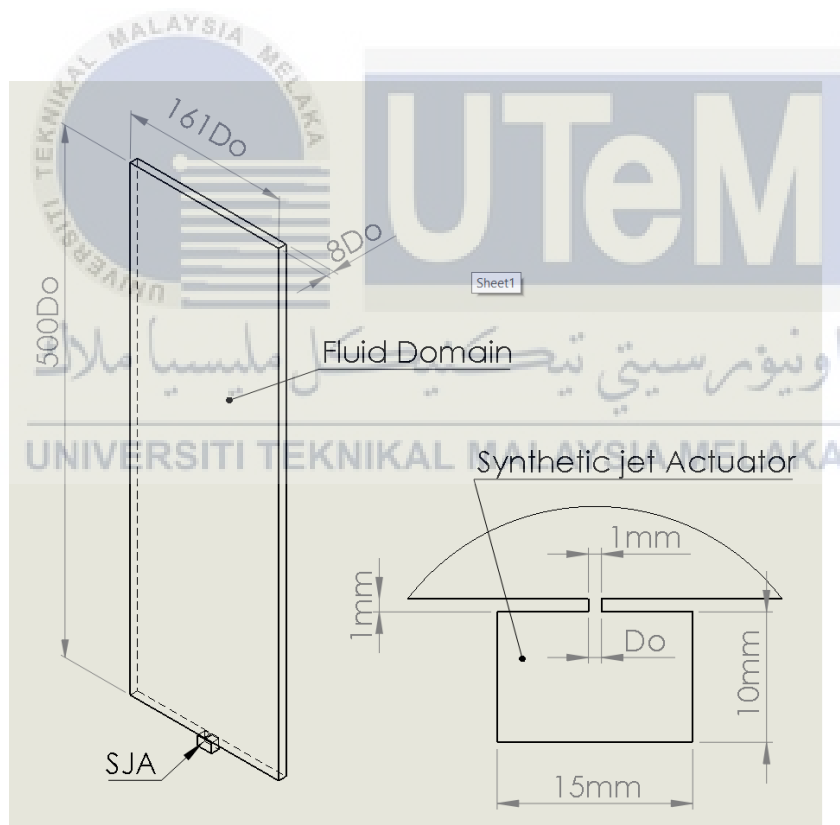


Figure 3.4: Dimension of synthetic jet actuator model

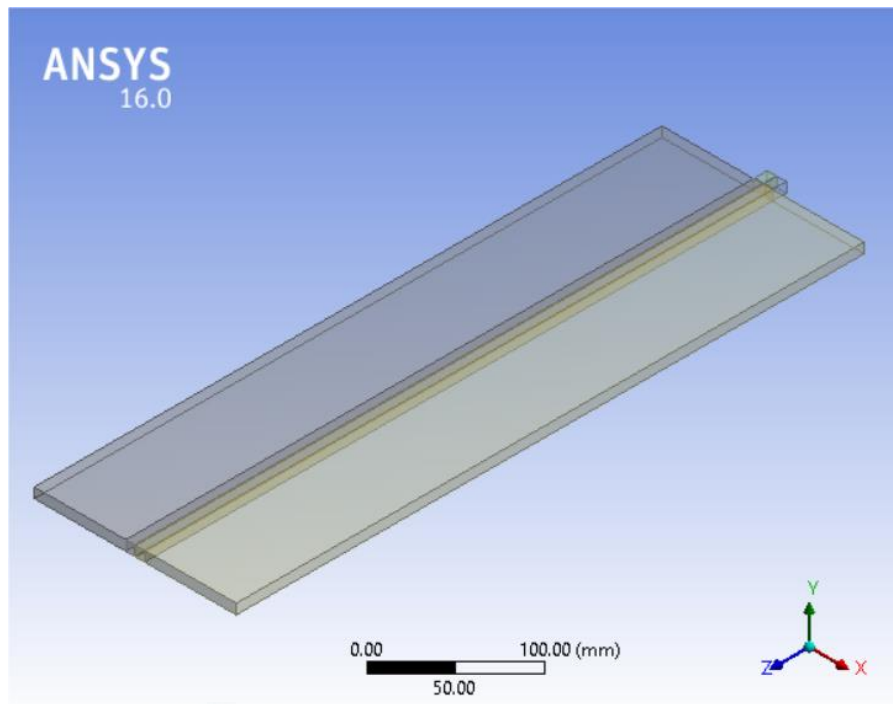


Figure 3.5: Geometry of synthetic jet actuator model

3.2.2 Meshing

After the geometry creation, the meshing of the synthetic jet model was done with structured hexagonal mesh of 3.55×10^5 mesh elements. The meshing was created with minimum orthogonal quality and maximum skewness of 1 and 1.312×10^{-10} respectively. The present mesh of the synthetic jet actuator model was shown in Figure 3.6. After meshing was done, the boundary condition of the synthetic jet actuator model was set which can be shown in Figure 3.7.

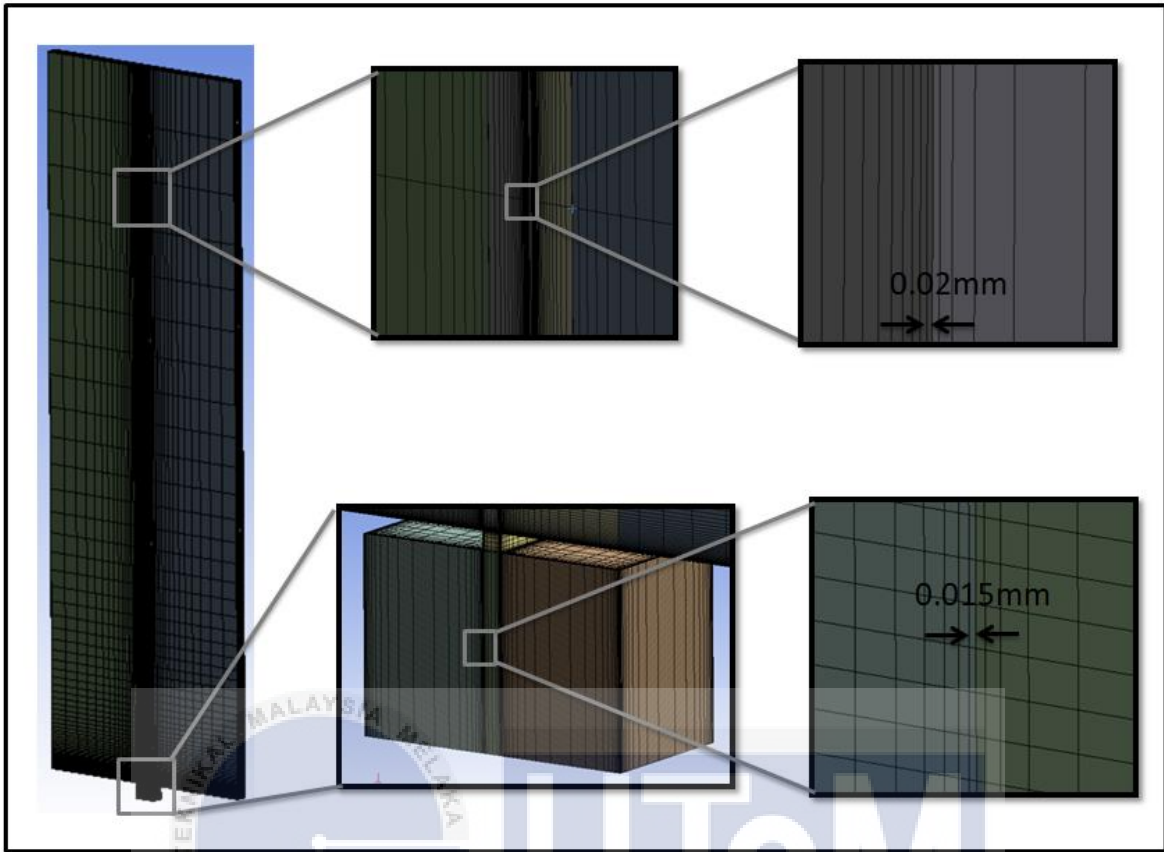


Figure 3.6: Mesh of synthetic jet actuator model

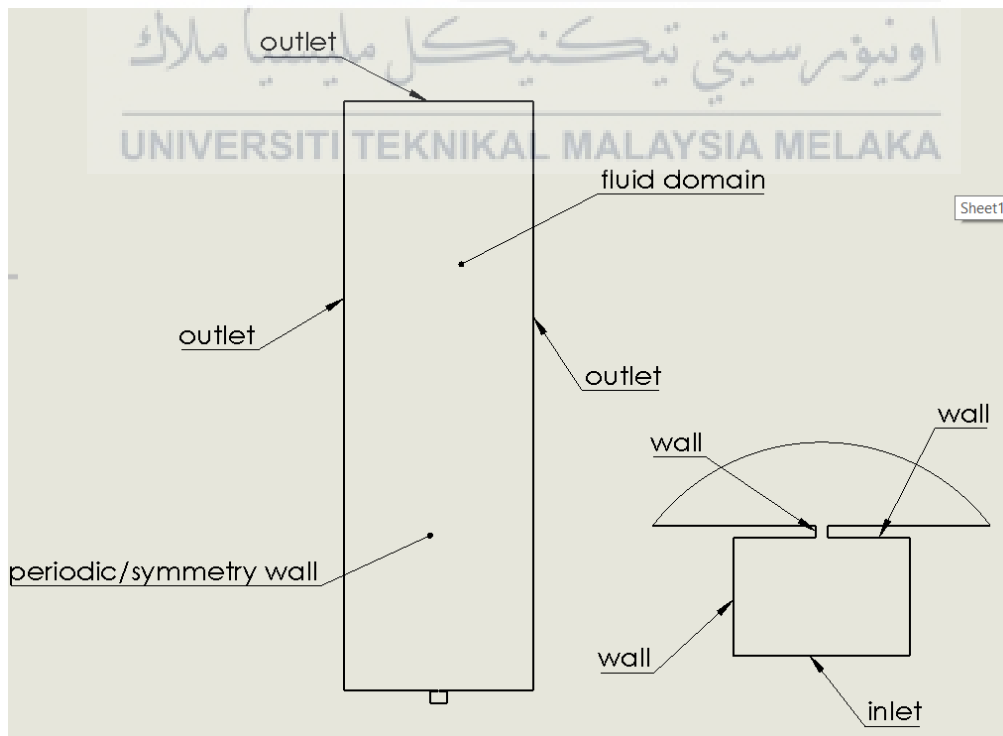


Figure 3.7: Boundary condition of the fluid domain (left) and synthetic jet actuator (right)

3.2.3 Fluent Setting

For the computational flow configuration of the SJA model, an incompressible laminar Reynolds-Average Navier-Stokes (RANS) equation was used in the fluent solver with the fluid density and viscosity of 1.238 kg/m^3 and $1.47 \times 10^{-5} \text{ kg/ms}$ respectively. The solid material of the simulations was set to be aluminium with density, specific heat and thermal conductivity of 2719 kg/m^3 , 871 J/kg.K and 202.4 W/m.K respectively. A transient PISO second order upwind scheme was used and the velocity of the fluid flow was generated by the oscillating inlet cavity wall with equation

$$z_{cavity\ wall} = A \cdot \sin(2\pi ft) \quad (3.1)$$

where the amplitude of the cavity wall, $A = 0.00041$ and frequency of the oscillation, $f = 1000 \text{ Hz}$. Besides, the time step size of the simulation was set to be 8.3333×10^{-6} and the user-defined function (UDF) of the cavity wall motion used in the layering dynamic mesh was shown in Figure 3.8. In the simulation, the absolute convergence criteria of the simulations were set as 1×10^{-3} .

```

#include "udf.h"
#define A 0.00041
#define PI 3.141592654
#define fre 1000.0

DEFINE_GRID_MOTION(fleximembrane, domain, dt, time, dtime)
{
  Thread *tf = DT_THREAD (dt);
  face_t f;
  Node *node_p;
  real xini, x, B;
  int n;

  SET_DEFORMING_THREAD_FLAG (THREAD_T0 (tf));

  begin_f_loop (f, tf)
  {
    f_node_loop (f, tf, n)
    {
      node_p = F_NODE (f, tf, n);

      if (NODE_POS_NEED_UPDATE (node_p))
      {
        NODE_POS_UPDATED (node_p);

        xini = 0.0;
        B = sin(2.0*PI*fre*time);
        x = A*B;
        NODE_Z (node_p) = xini + x;
      }
    }
  }
  end_f_loop (f, tf);
}

```

Figure 3.8: User-defined function of the cavity wall motion

3.2.4 Validation and verification

The validation of the SJA model was done by comparison of the simulation result with the time-averaged velocity distributions graph from Okada's paper. Besides, the verification was done on sensitivity test of different domain size, time step size and boundary condition. The three different domain size were $161D_0$ (original), $181D_0$ and $201D_0$ where $D_0 = 1\text{mm}$. Then, the sensitivity test were done on three different time step size which were 8.33×10^{-6} (120 time step per cycle (original)), 5.56×10^{-6} (180 time step per cycle) and 4.17×10^{-6} (240 time step per cycle). Lastly, different boundary condition such as periodic boundary condition and symmetry boundary condition were also chosen as one of the sensitivity test. All the sensitivity test results were presented by using the graphical method. The sensitivity test was done only on the z-velocity at the orifice exit because the

z-velocity is the most importance factor that a SJA needed in order to bombard the boundary layer to control the fluid flow.

3.2.4.1 Validation result

The validation of the synthetic jet actuator model was done by comparing the results of the time-averaged velocity distributions graph of both experiment and computational model at 9.8mm in the z-direction (Fig. 3.9). The time averaged z-velocity w is normalized by with the time-averaged z-velocity at the centerline of the orifice exit, w_{cl} while the horizontal x-axis position was normalized with the jet half width, x_b .

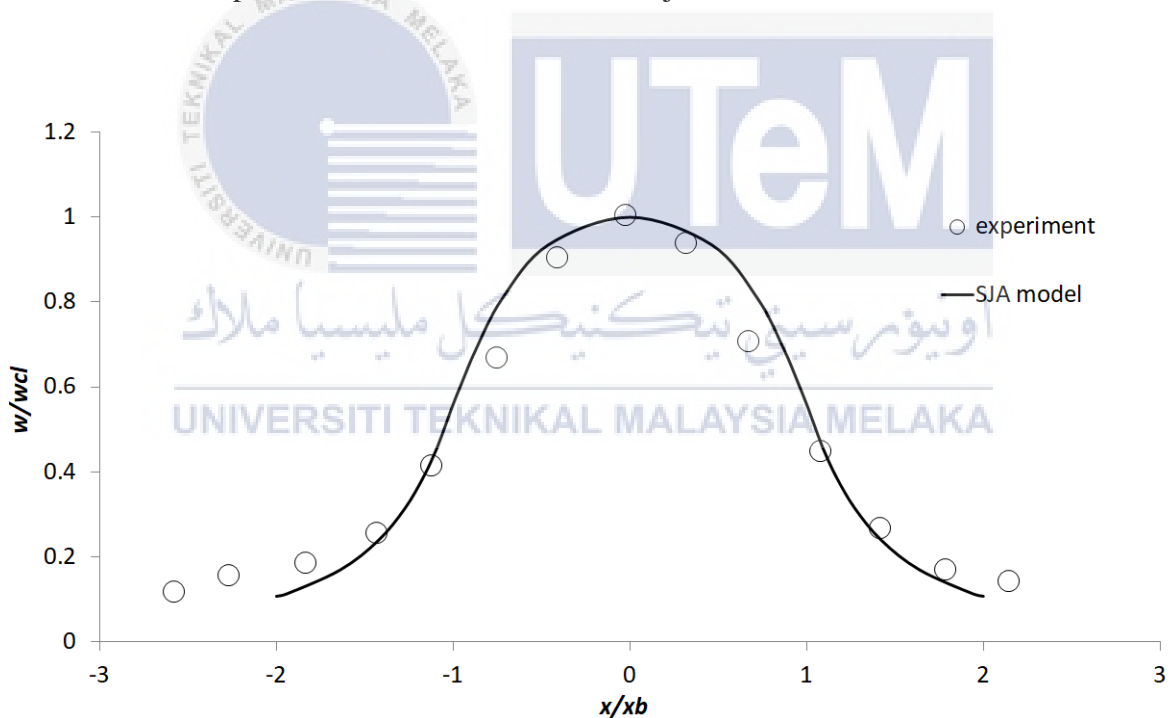


Figure 3.9: Comparison of the time-averaged velocity distributions between experiment results and synthetic jet actuator model at $z = 9.8\text{mm}$

3.2.4.2 Sensitivity test on different domain size

The sensitivity test of the effect of different domain size on z-velocity at orifice exit was conducted by using three different domain sizes which the $161D_o$ (original), $181D_o$ and

201D_o where D_o = 1mm. The simulation results showed that by using increasing the domain size to 181D_o and 201D_o, the graph of z-velocity against flow time shows no different compared to the original domain size with 161D_o (Fig. 3.10). Besides, the percentage difference of the z-velocity at the orifice exit is less than 1% compared to the 161D_o (original) domain size. Therefore, this shows that increasing the domain size does not have much effect on the simulation results.

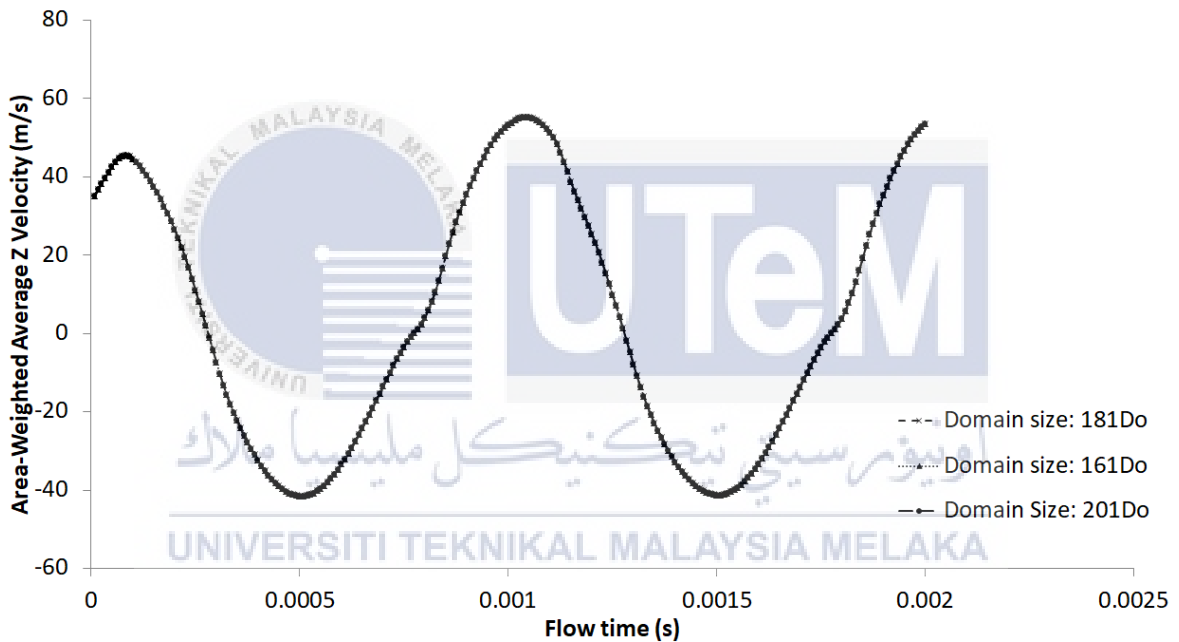


Figure 3.10: Graph of average z-velocity versus flow time at orifice exit for domain size 161D_o, 181D_o and 201D_o

3.2.4.3 Sensitivity test on different time step size

The sensitivity test for the effect of different time step size on the z-velocity at the orifice exit conducted with three different time step size which were 8.33×10^{-6} (120 time step per cycle (original)), 5.56×10^{-6} (180 time step per cycle) and 4.17×10^{-6} (240 time step per cycle). The time step size was calculated by using the following equation:

$$\text{time step size} = \frac{1}{f \cdot N}, \quad N = 120, 180, 240 \quad (3.2)$$

where N is the time step per cycle and f is the frequency of the cavity wall oscillation which is 1000Hz. The simulation results showed that by increasing the time step size to 5.56×10^{-6} and 4.17×10^{-6} , the graph of average z-velocity versus flow time showed no difference compared to the original time step size with 8.33×10^{-6} (Fig. 3.11). Besides, the percentage difference of the z-velocity at the orifice exit for both 5.56×10^{-6} and 4.17×10^{-6} time step size is less than 1% compared to the original time step size of 8.33×10^{-6} . Therefore, the results show that increasing the time step size does not have much effect on the simulation results.

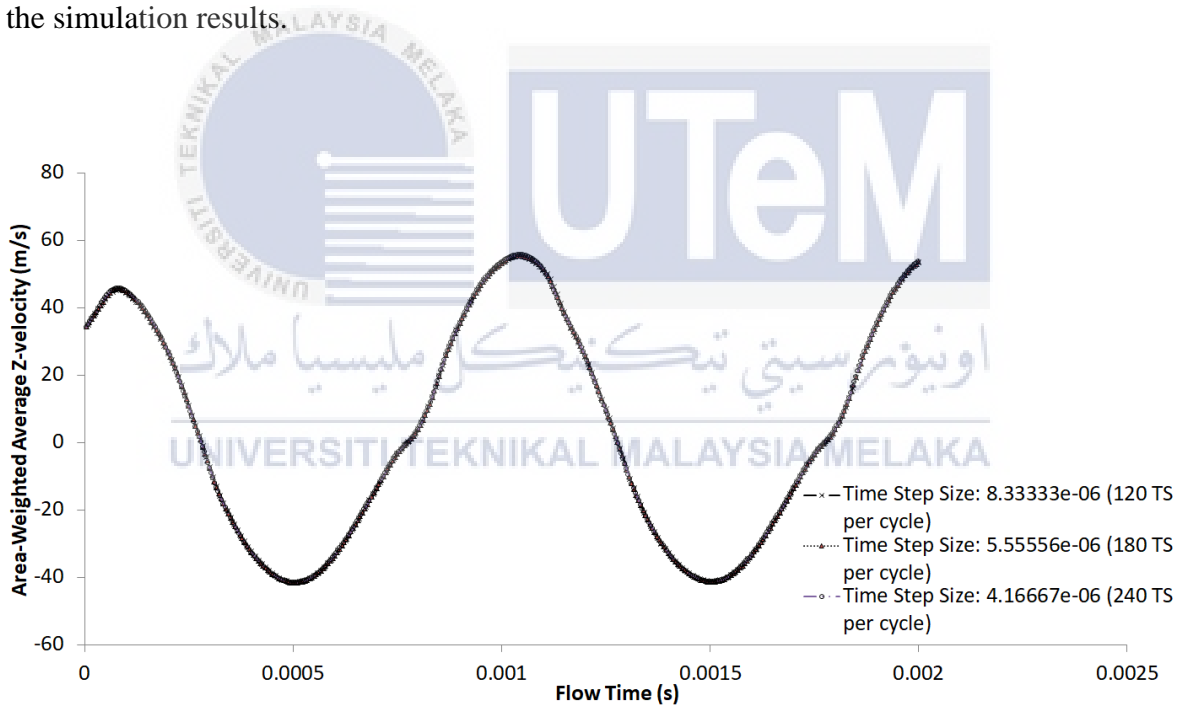


Figure 3.11: Graph of average z-velocity versus flow time at orifice exit for time step size 8.33×10^{-6} (120 time step per cycle), 5.56×10^{-6} (180 time step per cycle) and 4.17×10^{-6} (240 time step per cycle)

3.2.4.4 Sensitivity test on different boundary condition

For the similarity test on the effect of periodic boundary condition (original) and symmetry boundary condition on the z-velocity at orifice exit, the graph of average z-velocity versus flow time (Fig. 3.12) and velocity distribution at the orifice exit (Fig. 3.13) showed no significant difference among both boundary conditions. The percentage difference for the z-velocity at the orifice exit for symmetry boundary condition is less than 1% compared to the periodic boundary condition. Therefore, this showed that by changing the periodic boundary condition to symmetry boundary condition does not have much effect on the simulation results.

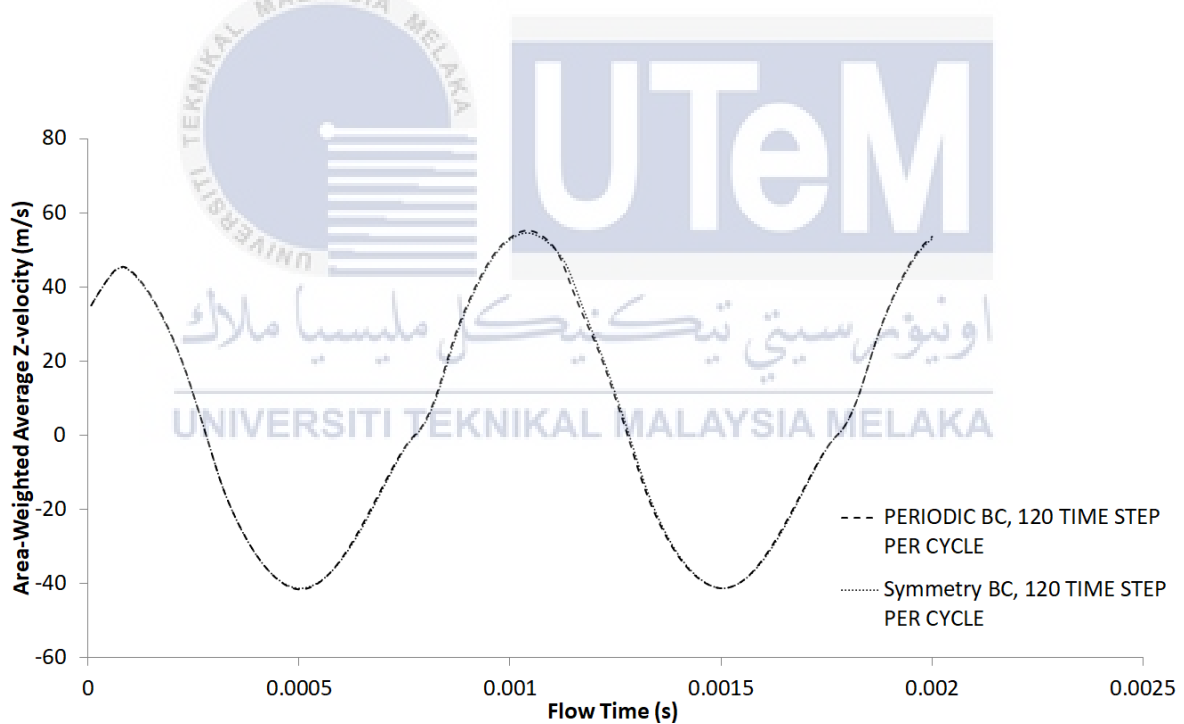


Figure 3.12: Graph of average z-velocity versus flow time at orifice exit for periodic boundary condition and symmetry boundary condition

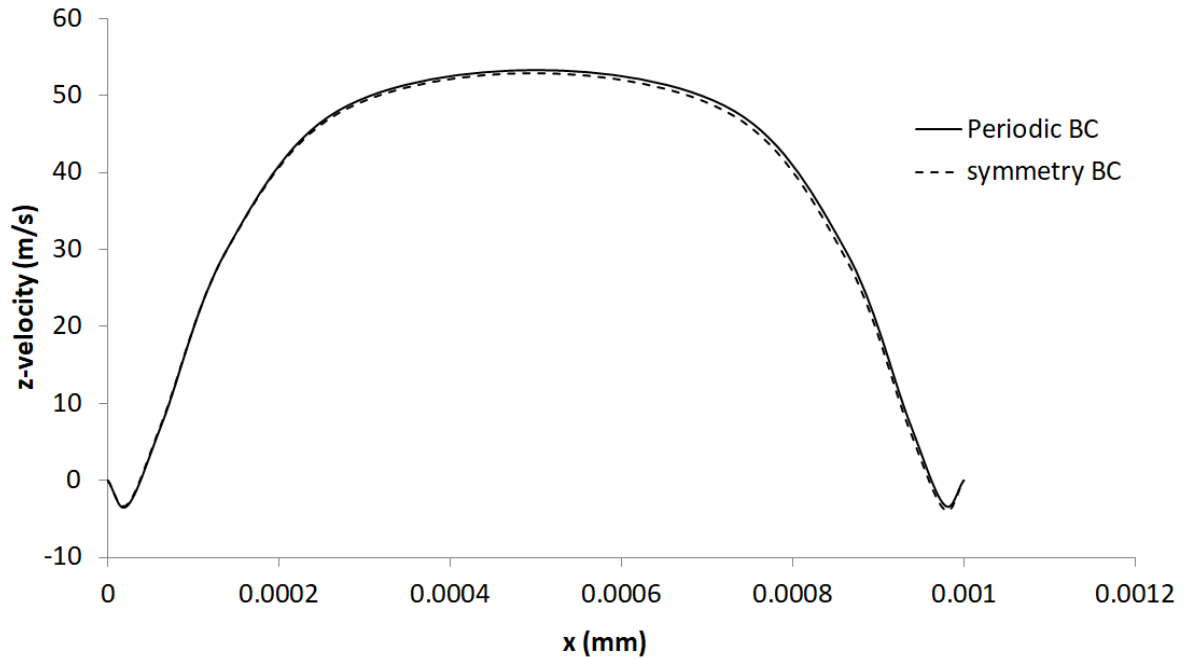


Figure 3.13: Graph of z-velocity versus x-axis position at orifice exit for periodic boundary condition and symmetry boundary condition

3.3 Flow in Backward-facing Step

The backward-facing step model was created to study the effect of the synthetic jet actuator location on the aerodynamic drag of the bluff body.

3.3.1 Geometry

The dimension of the backward-facing step was shown in Figure 3.14. The slope of the rounded backward-facing step was created by using the shape equation below:

$$\frac{y}{h} = \frac{1}{2\pi} \left(\sin \frac{0.703\pi x}{h} - \frac{0.703\pi x}{h} \right), \quad \frac{x}{h} \in \left[0, \frac{2}{a} \right] \quad (3.3)$$

which $h = 20\text{mm}$ (Dandois J. et al 2006). The backward-facing step has a length of $16h$ the $6h$ height from the slope. The geometry of the backward-facing step was created as shown in Figure 3.15.

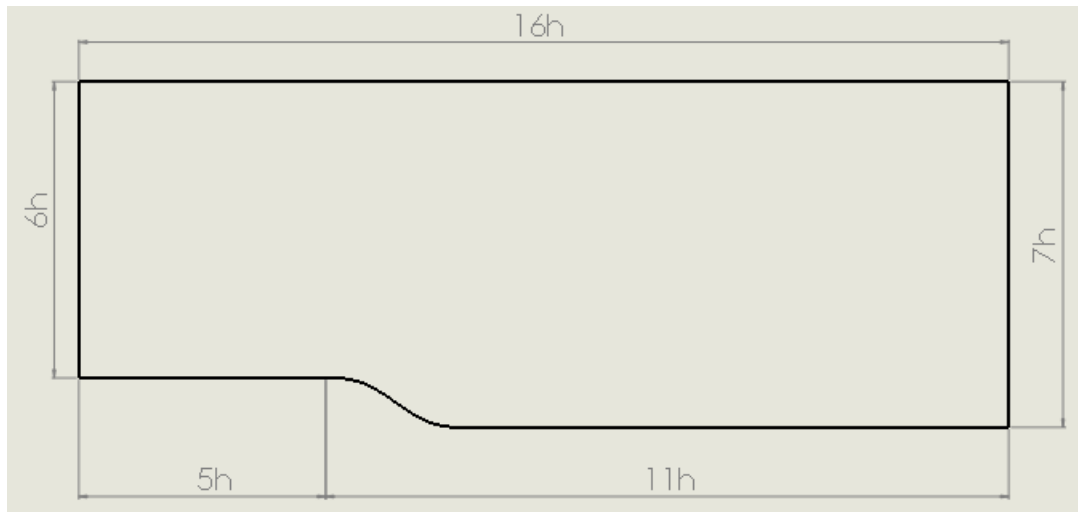


Figure 3.14: Dimension of backward-facing step model

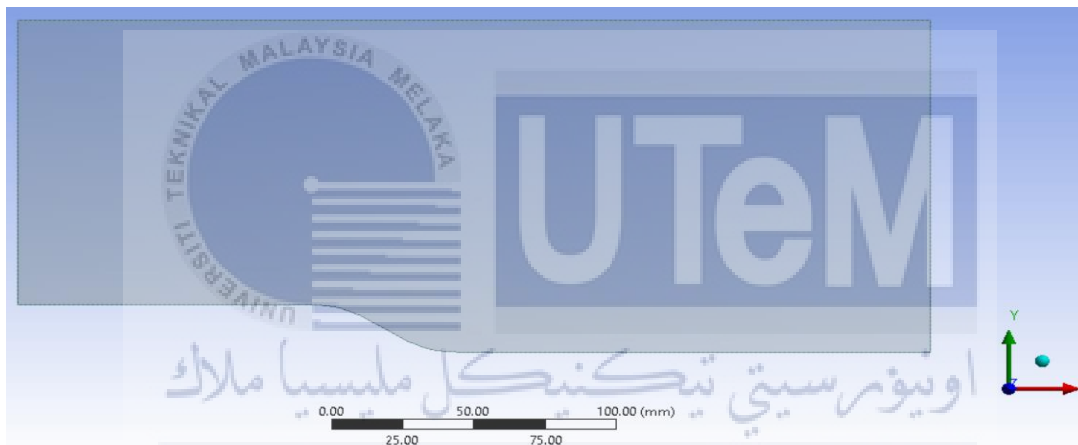


Figure 3.15: Geometry of backward-facing step

3.3.2 Meshing

The meshing of the backward-facing step was created by using structured hexagonal mesh cell with around 8100 elements. The minimum orthogonal quality and average skewness of the mesh were 0.82184 and 0.038427 respectively. The present mesh and the boundary condition of the backward-facing step were shown in the Figure 3.16 and Figure 3.17 respectively.

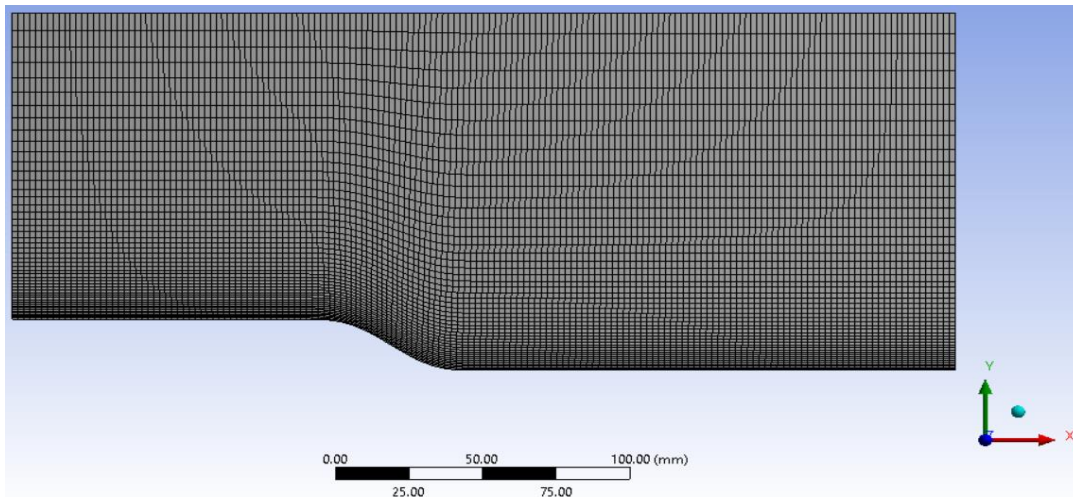


Figure 3.16: Mesh of backward-facing step

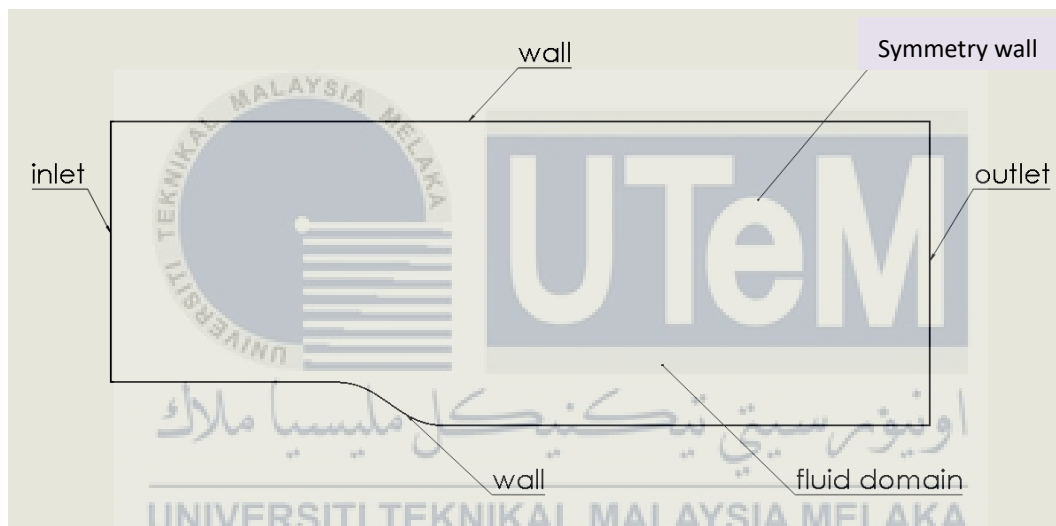


Figure 3.17: Boundary condition of the backward-facing step

3.3.3 Fluent setting

In the computational flow configuration of the backward-facing step for both uncontrolled and controlled case, the Mach number of the inlet stream was set to be subsonic with value of 0.3 and velocity of 101.133 m/s. The stagnation pressure and stagnation temperature were 20011 Pa and 283K respectively. The fluid density was set to be as ideal gas with fluid specific heat and thermal conductivity was set as 1006.43 J/kg.K and 0.0242W/m.K respectively. The solid material of the simulations was set to be aluminium with density,

specific heat and thermal conductivity of 2719kg/m³, 871 J/kg.K and 202.4W/m.K respectively. The viscosity of the fluid was set as two coefficient sutherland equation with constant C₁ and C₂ of 8.58x10⁻⁵ and 283 respectively. An unsteady compressible Spalart-Allmaras turbulence Reynolds-Average Navier-Stokes (URANS) equation was used in the fluent solver which the details for the numerical method can be refer to the work of Pechier et al. (2001) and Dandois J. et al. (2006). The time step of the simulations was taken to be 1x10⁻⁴ for the simulation. As for controlled flow with synthetic jet actuator, the inlet velocity profile of the synthetic jet actuator was generated by using the user-defined function in Figure 3.18 with the velocity equation of

$$v_{SJA} = v_{max} \cdot \cos(2\pi ft) \quad (3.3)$$

where the peak velocity of the synthetic jet, $v_{max} = 50\text{m/s}$ and frequency of the oscillation, $f = 720\text{Hz}$. The width of the orifice of the synthetic jet actuator was set to be 3.33mm. In the simulation, the absolute convergence criteria of the simulations were set as 1x10⁻³.

```
#include "udf.h"

#define PI 3.141592654

DEFINE_PROFILE(unsteady_velocity, thread, position)
{
    face_t f;
    real t = CURRENT_TIME;

    begin_f_loop(f, thread)
    {
        F_PROFILE(f, thread, position) = 50*cos(1440*PI*t);
    }
    end_f_loop(f, thread)
}
```

Figure 3.18: User-defined function of the synthetic jet velocity profile

3.3.4 Validation and verification

The validation and verification of the uncontrolled backward-facing step was done by comparing the current RANS model with the DNS model done by Dandois J. et al. (2006) by using uncontrolled backward-facing step model. In this validation process, the DNS model acts as a database to validate the RANS model. Besides, the verification process was done on the grid independency test of four different mesh elements to determine the most suitable mesh element for simulation.

3.3.4.1 Validation result

The result of the validation was shown in the graph of the evolution of the time-averaged streamwise velocity profile inside the backward-facing step (Fig. 3.19). The results showed that streamwise velocity profile of the RANS model was not perfectly match with the DNS model. The differences in streamwise velocity profile were caused by difference in model dimension in which the current case was using 2-dimensional model instead of using 3-dimensional model due to insufficient of computational time.

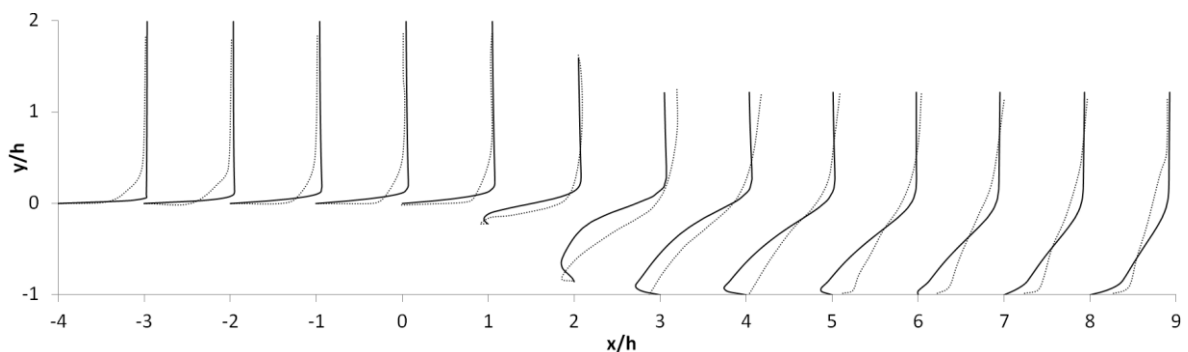


Figure 3.19: Time-averaged streamwise velocity $x/h + u/U_\infty$ (solid line: RANS, dotted line: DNS)

3.3.4.2 Grid independency test

In order to determine the mesh element was sufficient enough for the computational process, a grid independency test was done by using four differences number of mesh cells which were 4050 mesh cells, 8100 mesh cells, 10750 mesh cells and 16050 mesh cells (Fig. 3.20 and Fig. 3.21). The drag coefficients of four different mesh cells were listed in Table 3.1. From Table 3.1, the average drag coefficient between 4050 mesh cells and 8100 mesh cells showed significant difference with 85.71% difference in drag coefficient while the average drag coefficient showed no significant difference with only 14.29% difference when increased the mesh cells to 10750 mesh cells and 16050 mesh cells. Therefore, the mesh cell used was suggested to be 8100 mesh cells in order to minimize the computational time.

Table 3.1: Drag coefficient of different mesh cells

Number of mesh cells	Average Drag Coefficient, C_D	Percentage increase in mesh cell (%)
4050	6.94×10^{-3}	-50.00
8100	7.00×10^{-3}	-
10750	7.01×10^{-3}	32.71
16050	7.02×10^{-3}	98.15

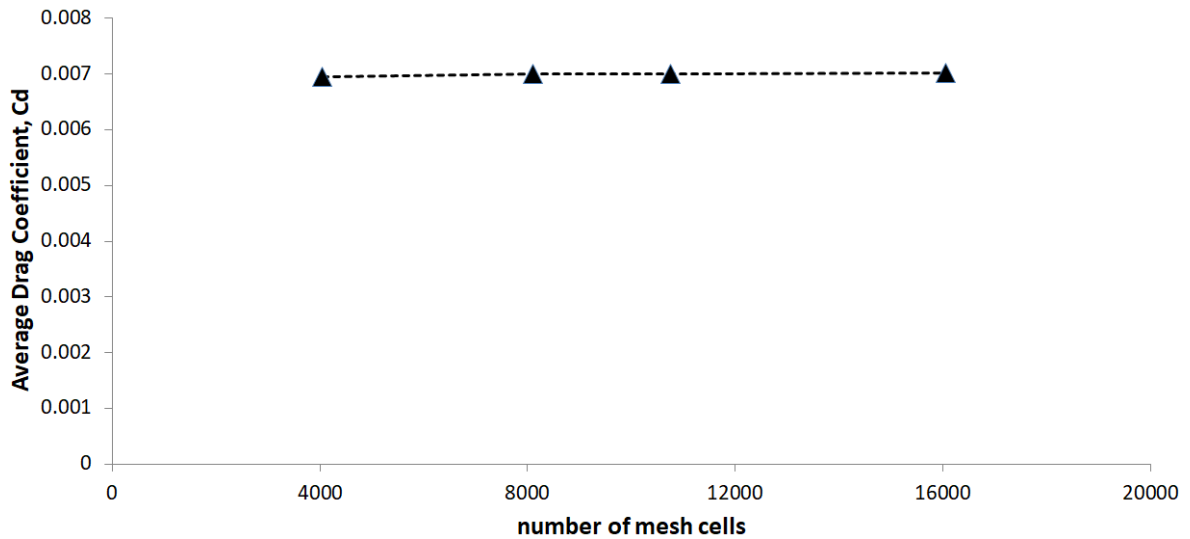


Figure 3.20: Graph of average drag coefficient at slope versus number of mesh cells

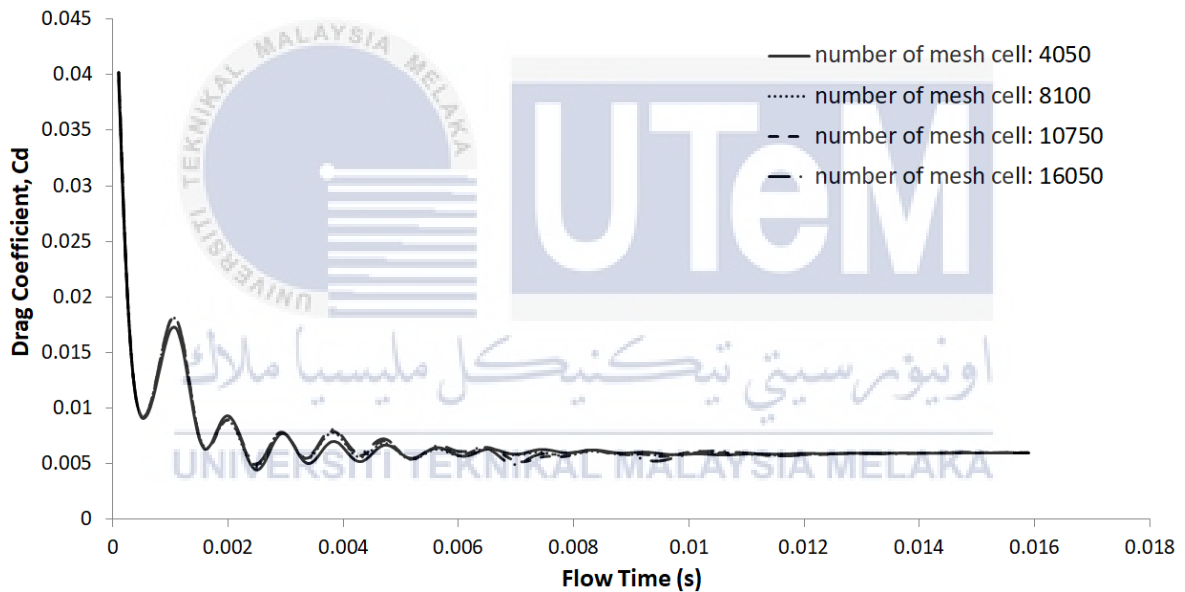


Figure 3.21: Graph of drag coefficient versus flow time at the slope for four different mesh cells

3.3.5 Result comparison

After the simulation in ANSYS, the results from the fluid flow simulation were visualised in contour and graphical method in order to do the results comparison. In this project, the result comparison for the backward-facing step was done on the three different position of the synthetic jet actuator at the backward-facing step which was at the upstream,

downstream and directly at the separation point. Besides, the results of placing two synthetic jet actuators on the separation point and reattachment point respectively was compared with the result of placing single synthetic jet actuator at the upstream, downstream and directly at the separation point.



CHAPTER 4

RESULTS AND DISCUSSIONS

4.1 Synthetic Jet Actuator Location in the Backward-facing Step for All Cases

In this project, the simulation of 5 different cases was conducted in which 4 of them are controlled flow cases which were conducted by placing the synthetic jet actuator at different locations which shown in Table 4.1. The SJA location was set up based on the separation point from the simulation results of the uncontrolled flow cases which shown in Figure 4.1. From the simulation, the position of the separation point of the flow was determined to be at $x = 15.7$ mm. After that, the location of the synthetic jet actuator at the reattachment point in Case 4 was determined by using the simulation results of Case 1 which can be shown in streamline profile in Figure 4.2.

Table 4.1: All Computational Cases

Case	Description	Location of SJA
0	Uncontrolled flow	None
1	SJA located at separation point	$0.75h$
2	SJA located before separation point	$0.25h$
3	SJA located after separation point	$1.25h$
4	SJA array located at separation and reattachment point of Case 1	$0.75h$ and $2.0825h$

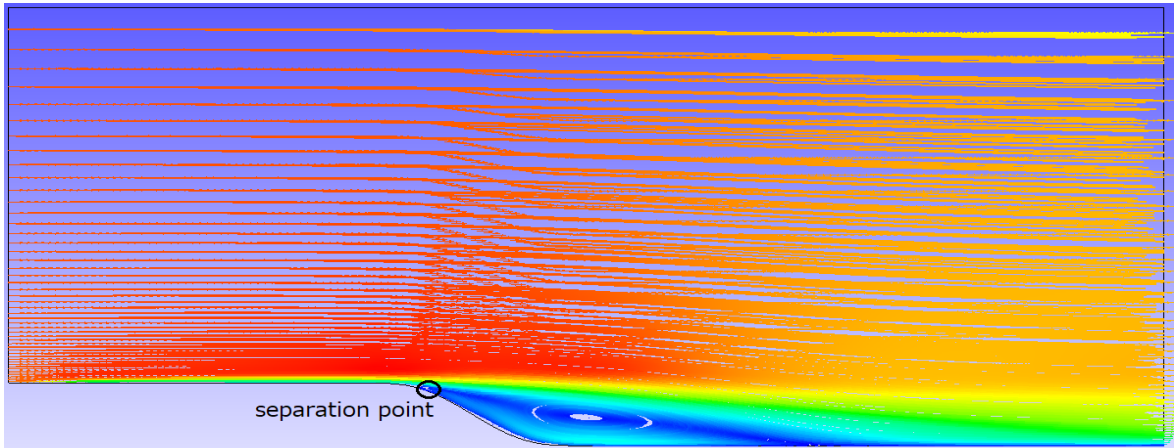


Figure 4.1: Streamline profile of the uncontrolled flow case (Case 0) and the location of the separation point

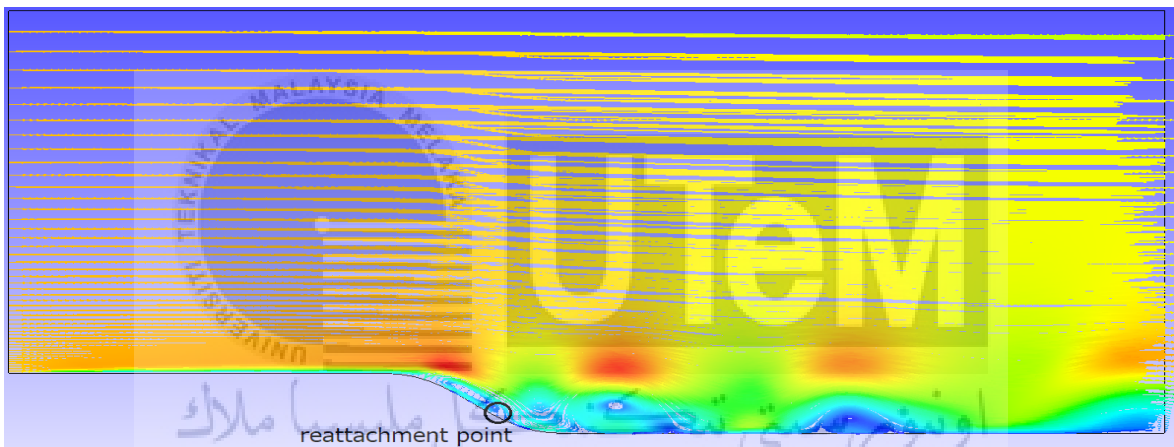


Figure 4.2: Streamline profile of the controlled flow case (Case 1) and the location of the reattachment point

4.2 Effect of the Synthetic Jet Actuator Location in the Backward-facing Step on the Aerodynamic Drag

The graph of the drag coefficient, C_D and lift coefficient, C_L versus flow time was plotted for all cases which can be shown in Figure 4.3 and Figure 4.4. The average value of the drag coefficient, lift coefficient and lift-to-drag ratio were recorded in Table 4.2. For the controlled case with only one synthetic jet actuator which were case 1, case 2 and case 3, the percentage of drag reduction increase from case 2 to case 3 and then followed by case 1.

Besides that, the controlled case with two synthetic jet actuators (Case 4) had the highest drag reduction compared to all other cases. For lift coefficient, the lift reduction was the highest in case 2 followed by case 1, case 4 and case 3. For overall performance, case 4 had the best performance as the lift-to-drag ratio was the highest. Although all the case had reduction in both drag and lift, case 1 and case 2 had lower performance compared to the case 0 which was without SJA. The reduction of the drag force and lift force was highly related to the size of the separation bubble (Tani et al. 1964) and the location of the separation point.

Table 4.2: Aerodynamic properties of all cases

Case	C_D	ΔC_D (%)	C_L	ΔC_L (%)	C_L / C_D
0	0.00595	-	0.0172	-	2.891
1	0.00490	-17.647	0.0134	-22.093	2.735
2	0.00590	-0.840	0.0132	-23.256	2.237
3	0.00532	-10.588	0.0168	-2.326	3.158
4	0.00440	-26.050	0.0144	-16.279	3.273

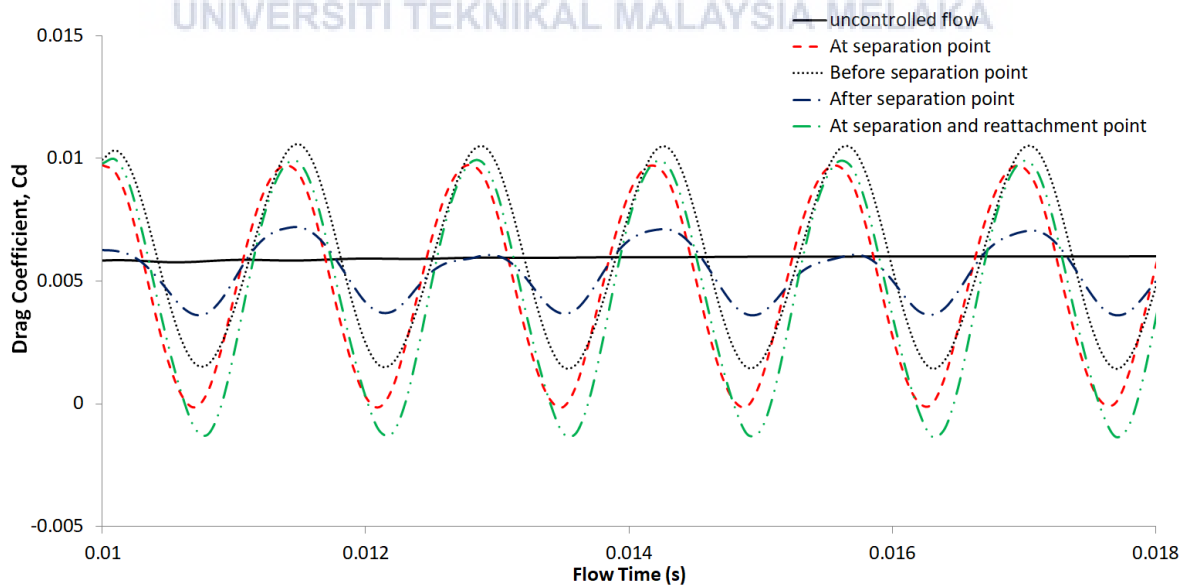


Figure 4.3 Graph of drag coefficient versus flow time at the slope for all cases

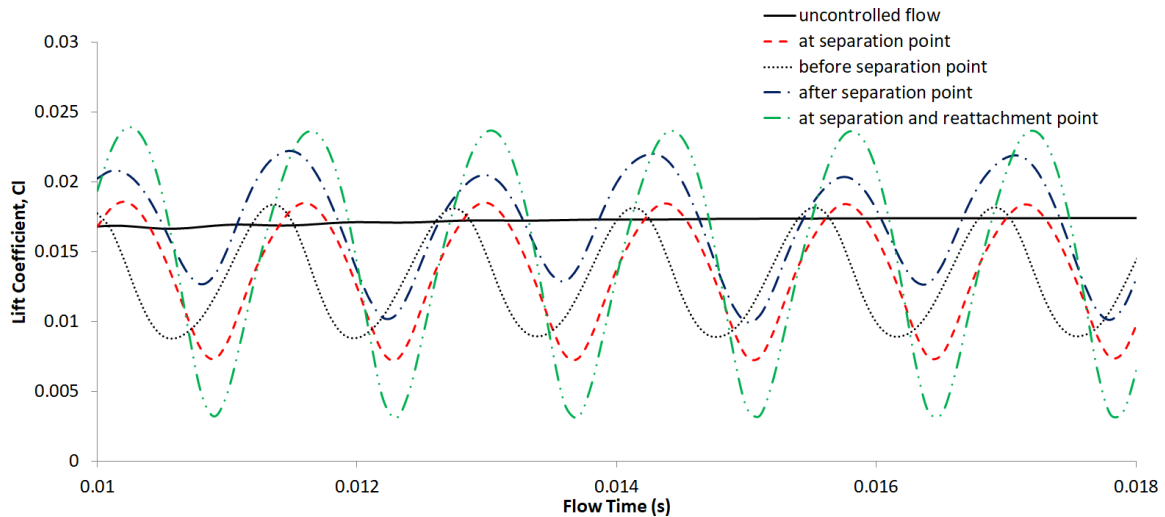


Figure 4.4: Graph of lift coefficient versus flow time at the slope for all cases

Table 4.3 showed the pressure force and viscous force for lift and drag of uncontrolled case (Case 0). From the simulation results in Table 4.3, the drag and lift force of the backward-facing step was highly caused by the pressure force rather than viscous force. This is because the value of the viscous force is significantly small which can be ignored. The pressure drag force was built up by the formation of the separation bubble at the slope where the adverse pressure gradient built up when the air flow by. Table 4.4 showed the properties of the separation bubble for all the computational cases. As can be seen in Figure 4.5, Figure 4.6 and Table 4.4, case 2 had the highest separation length among the controlled cases followed by case 3, case 1 and case 4. Although the separation length of case 3 is much longer than case 2, but due to the location of the separation point of case 3 is much further than case 2, the drag force of case 3 is lower than case 2. Besides that, the earliest separation bubble occurrence of case 2 caused the drag force of case 2 was the highest among other controlled cases. After that, case 4 had the shortest separation length compared to the others which caused it had the lowest drag. From the point view of

vorticity dynamics, the amount of energy gained by boundary layer was highly depend on the distance of the vortices to the surface (Swift. et al. 2009). From Figure 4.7, it can be seen that the vortex of the case 4 is further than the slope surface compare to case 1. This caused the drag force of case 4 is lower than case 1. As for case 2, the drag force is higher than other controlled cases because the strength of vorticity is larger near the slope surface as the green area is bigger than others which can be seen in Figure 4.7 (c).

Table 4.3: Drag and lift properties of uncontrolled case (Case 0)

Case	Pressure Drag, $F_{DP}(N)$	Viscous Drag, $F_{DV}(N)$	Pressure Lift, $F_{LP}(N)$	Viscous Lift, $F_{LV}(N)$
0	37.964	0.259	111.561	0.063

Table 4.4: Separation bubble properties of all cases

Case	x_s / h	x_r / h	L_{sep} / h	$\Delta L_{sep} (%)$
0	0.785	6.125	5.340	-
1	0.665	2.040	1.375	-74.251
2	0.165	1.770	1.605	-69.944
3	1.575	5.405	3.830	-28.277
4	0.665	1.908	1.243	-76.723

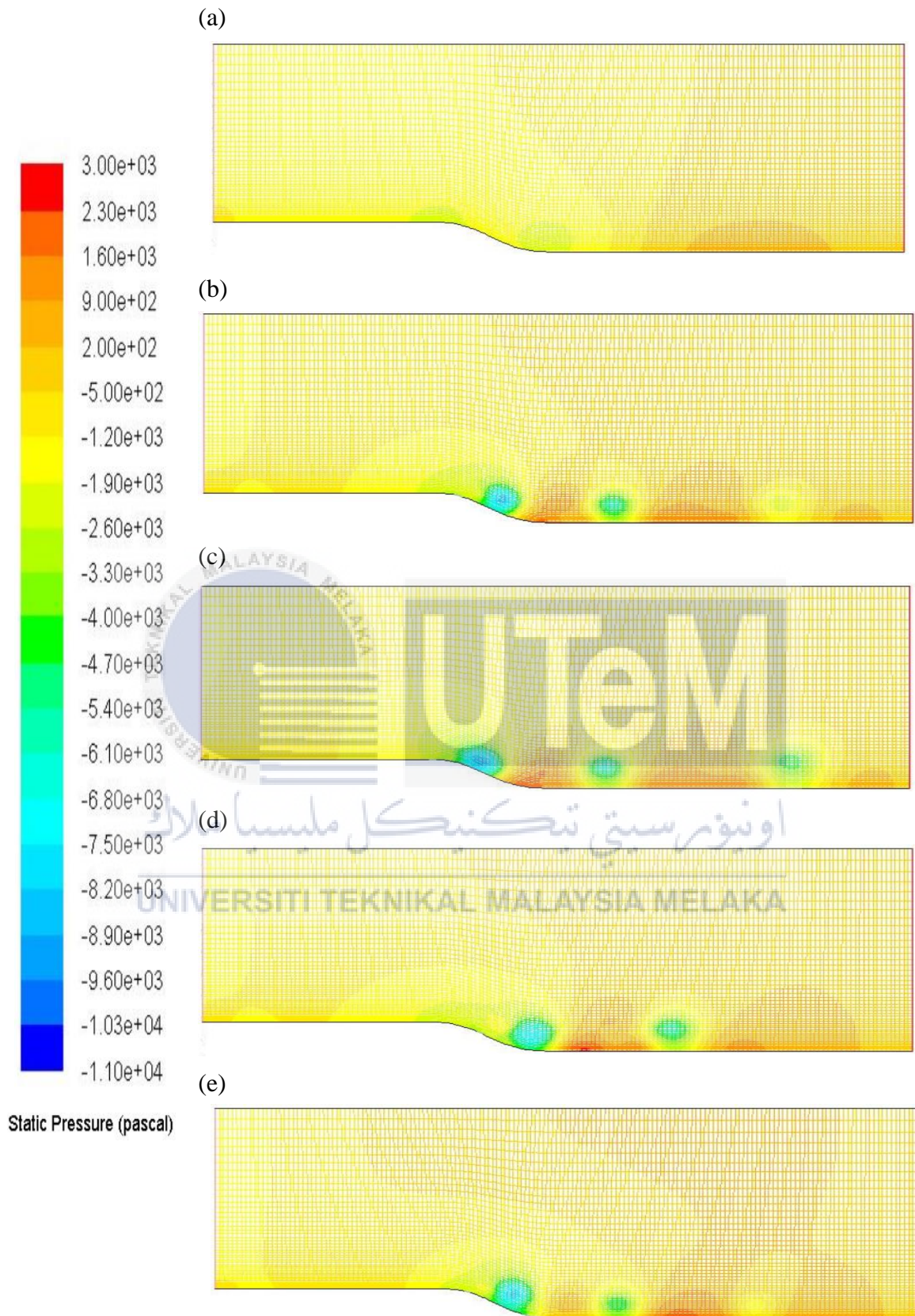


Figure 4.5: Pressure contour of all cases after blowing stroke at $t = 4.5 \times 10^{-3}$ s
 (a) Case 0 (b) Case 1 (c) Case 2 (d) Case 3 (e) Case 4

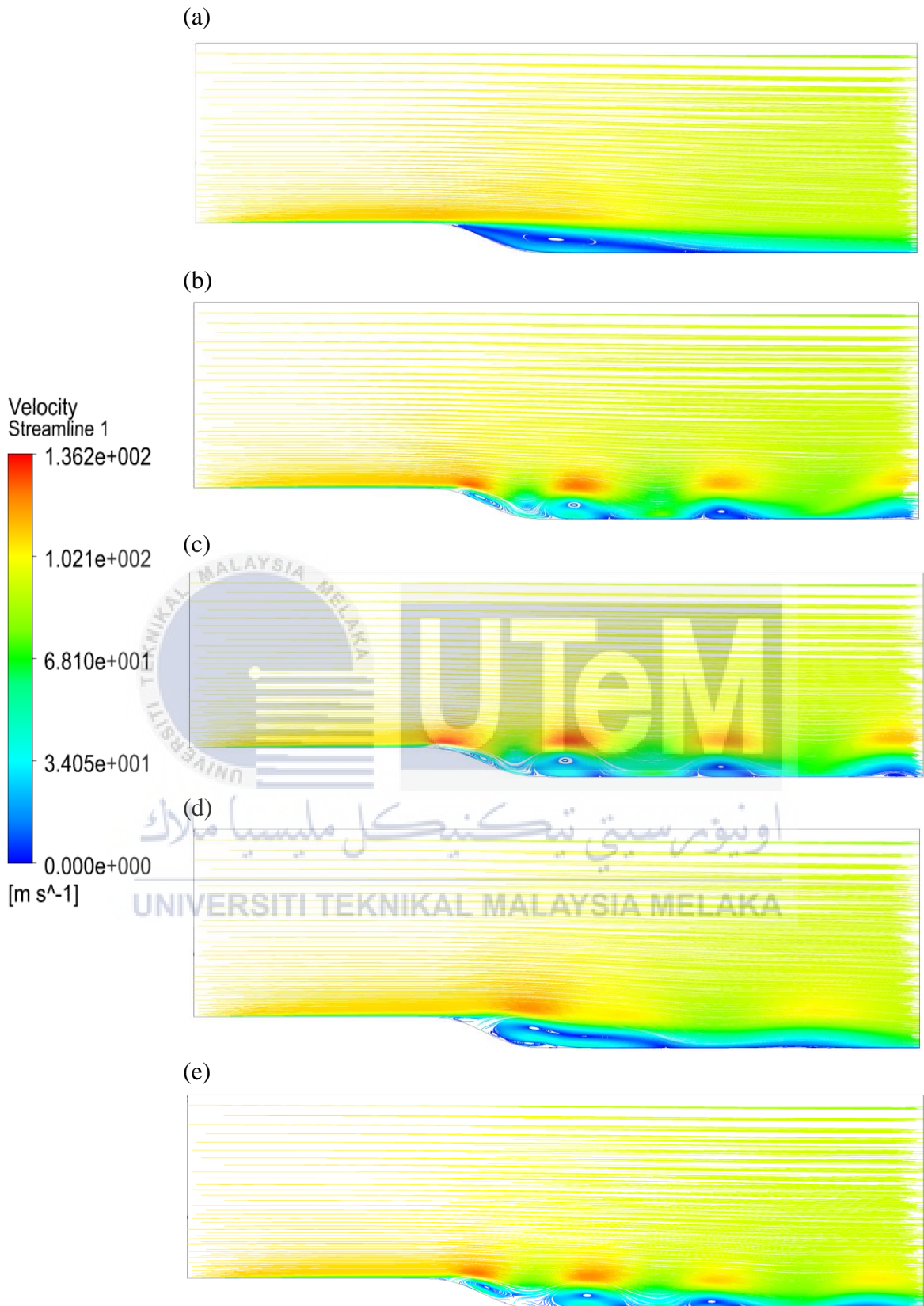


Figure 4.6: Streamline profile of all cases
 (a) Case 0 (b) Case 1 (c) Case 2 (d) Case 3 (e) Case 4

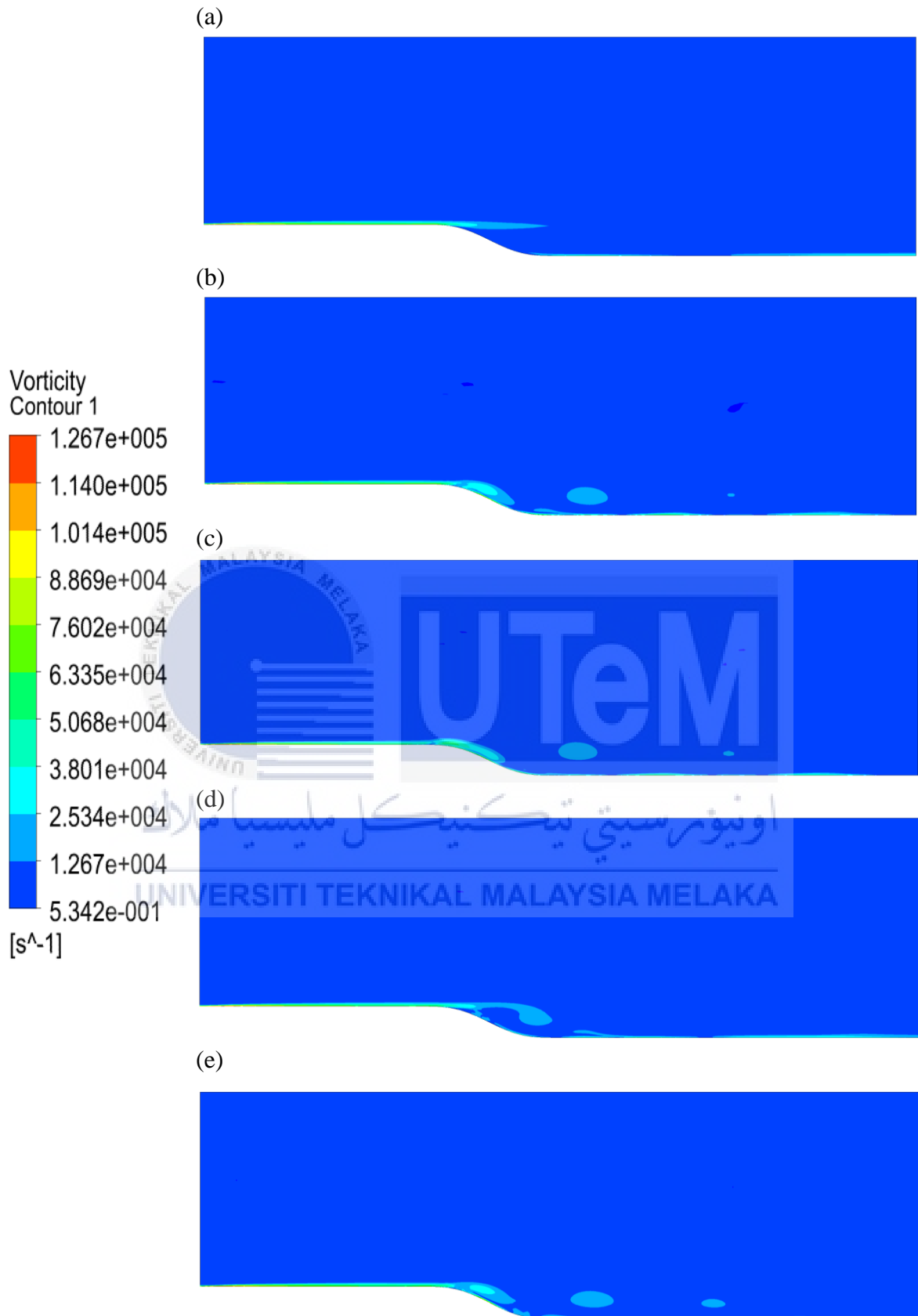


Figure 4.7: vorticity contour of all cases
 (a) Case 0 (b) Case 1 (c) Case 2 (d) Case 3 (e) Case 4

CHAPTER 5

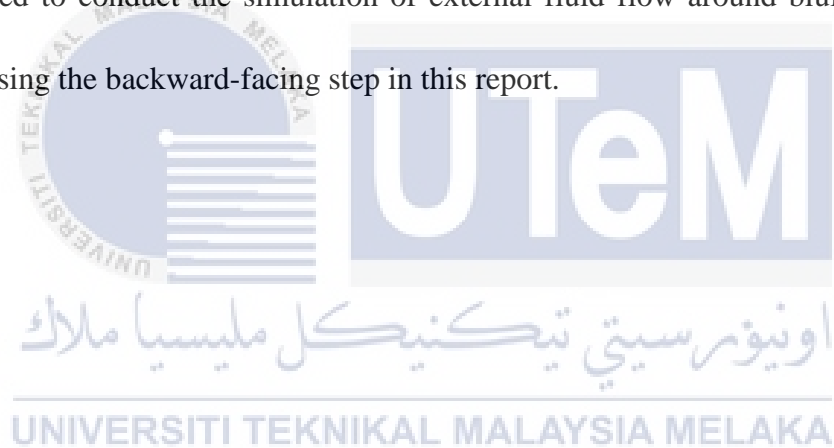
CONCLUSION AND RECOMMENDATIONS FOR FUTURE RESEARCH

In this project, the studied for two computational models was conducted by using CFD simulations in ANSYS Fluent software in which the simulations conducted for SJA model and backward-facing step model. The SJA was inserted into the backward-facing step at various locations to evaluate the effect of the SJA location on the aerodynamic drag. The simulation fluid flow was in turbulence condition with Mach number of 0.3. The locations for single SJA cases were at $0.25h$, $0.75h$ and $1.25h$ respectively whereas the locations for double SJA case were at $0.75h$ and $2.0825h$ respectively.

1. The separation length, lift and drag were reduced with the present of SJA in the backward-facing step.
2. For single SJA cases, the separation length decreased from SJA location at $1.25h$, $0.25h$ and $0.75h$. The separation length of the double SJA cases was the lowest compared to single SJA cases.
3. For single SJA cases, the drag reduced from $0.25h$, $1.25h$ and $0.75h$. The drag force of the double SJA cases was the lowest compared to single SJA cases.
4. The value of the drag force is depending on the separation point, vorticity and size of separation bubble at the slope. Longer separation length, earlier separation point and stronger vorticity near the surface will lead to higher drag force.

5. The ideal location to locate the SJA was at both separation and reattachment points same as case 4.

It is recommended that further study on the frequency of the separation bubble formation would be conduct to have a deeper understanding on the influence of the synthetic jet actuator on the drag and lift of the bluff body. Besides, the effect of the frequency of the SJA vibration diaphragm on the aerodynamic drag and lift of the bluff body should also be studied. Lastly, in order to have a more realistic result, it is recommended to conduct the simulation of external fluid flow around bluff body model instead of using the backward-facing step in this report.



REFERENCES

- Çengel, Y. A., & Cimbala, J. M. (2006). *Fluid mechanics: Fundamentals and applications*.
- Dandois, J., Garnier, E., & Sagaut, P. (2006). Unsteady Simulation of Synthetic Jet in a Crossflow. *AIAA Journal*, 44(2), 225-238. doi:10.2514/1.13462
- DANDOIS, J., GARNIER, E., & SAGAUT, P. (2007). Numerical simulation of active separation control by a synthetic jet. *Journal of Fluid Mechanics*, 574, 25. doi:10.1017/s0022112006003995
- Deng, X., Xia, Z., Luo, Z., & Wang, L. (2014). A novel optimal design for an application-oriented synthetic jet actuator. *Chinese Journal of Aeronautics*, 27(3), 514-520. doi:10.1016/j.cja.2014.04.002
- El-Ali, M., & Chalmers tekniska högskola. (2012). *Active flow control for drag reduction of heavy vehicles*.
- Feero, M. A., Lavoie, P., & Sullivan, P. E. (2015). Influence of cavity shape on synthetic jet performance. *Sensors and Actuators A: Physical*, 223, 1-10. doi:10.1016/j.sna.2014.12.004
- Fox, R. W., Pritchard, P. J., & McDonald, A. T. (2010). *Introduction to fluid mechanics*. Hoboken, NJ: Wiley.
- Harinaldi, Budiarto, Tarakka, R., Simanungkalit, S.P. (2011). Computational analysis of active flow control to reduce aerodynamics drag on a van model. *International Journal of Mechanical & Mechatronics Engineering*, vol 11, 24-30.

- He, Y., Cary, A., & Peters, D. (2001). Parametric and dynamic modeling for synthetic jet control of a post-stall airfoil. *39th Aerospace Sciences Meeting and Exhibit*. doi:10.2514/6.2001-733
- Houghton, E. L., Carpenter, P. W., & Collicott, S. (2012). *Aerodynamics for Engineering Students 6th edition*.
- Javaherci, T. (2010). *Review of Spalart-Allmaras Turbulence Model and its Modification*.
- Kotapati, R., Mittal, R., & Cattafesta, L. (2006). Numerical Experiments in Synthetic Jet Based Separation Control. *44th AIAA Aerospace Sciences Meeting and Exhibit*. doi:10.2514/6.2006-320
- Konstantinidis, E., & Bouris, D. (2016). Vortex synchronization in the cylinder wake due to harmonic and non-harmonic perturbations. *Journal of Fluid Mechanics*, 804, 248-277. doi:10.1017/jfm.2016.527
- Krishnappa, S., & Embry-Riddle Aeronautical University. (2016). *An experimental study of synthetic jet actuators with application in airfoil LCO control*.
- Laha D. (2015). *Computational aerodynamics analysis of a rear spoiler on a car in two dimensions*. United Kingdom: Anglia Ruskin University.
- Langtry, R., Menter, F. (2006). *Overview of Industrial Transition Modelling in CFX*, Germany: ANSYS.
- Lee, C., Woyciekoski, M., & Copetti, J. (2016). Experimental study of synthetic jets with rectangular orifice for electronic cooling. *Experimental Thermal and Fluid Science*, 78, 242-248. doi:10.1016/j.expthermflusci.2016.06.007

- Lv, Y., Zhang, J., Shan, Y., & Tan, X. (2014). Numerical investigation for effects of actuator parameters and excitation frequencies on synthetic jet fluidic characteristics. *Sensors and Actuators A: Physical*, 219, 100-111. doi:10.1016/j.sna.2014.08.009
- Marcin Kurowski & Piotr Doerffer (2015). Influence on membrane amplitude and forcing frequency on synthetic jet velocity. *Task Quarterly vol 19*, 2, 111-12.
- Mello, H. C., Catalano, F. M., & Souza, L. F. (2007). Numerical study of synthetic jet actuator effects in boundary layers. *Journal of the Brazilian Society of Mechanical Sciences and Engineering*, 29(1), 34-41. doi:10.1590/s1678-58782007000100006
- Montazer, E., Mirzaei, M., Salami, E., Ward, T. A., Romli, F. I., & Kazi, S. N. (2016). Optimization of a synthetic jet actuator for flow control around an airfoil. *IOP Conference Series: Materials Science and Engineering*, 152, 012023. doi:10.1088/1757-899x/152/1/012023
- Murugan, T., Deyashi, M., Dey, S., Rana, S. C., & Chatterjee, P. (2016). Recent Developments on Synthetic Jets (Review Paper). *Defence Science Journal*, 66(5), 489. doi:10.14429/dsj.66.9776
- OBERKAMPF, W. L., & TRUCANO, T. G. (2002). Verification and Validation in Computational Fluid Dynamics. doi:10.2172/793406
- Okada, K., Oyama, A., Fujii, K., & Miyaji, K. (2010). Computational Study on Effect of Synthetic Jet Design Parameters. *International Journal of Aerospace Engineering*, 2010, 1-11. doi:10.1155/2010/364859

- Pechier, M., Guillen, P., & Cayzac, R. (2001). Magnus Effect over Finned Projectiles. *Journal of Spacecraft and Rockets*, 38(4), 542-549. doi:10.2514/2.3714
- Saambavi, K., & Embry-Riddle Aeronautical University. (2014). *Flow separation control using synthetic jets on a flat plate*. Daytona Beach, FL: Embry-Riddle Aeronautical University.
- Schlesinger, S. (1979). Terminology for model credibility. *SIMULATION*, 32(3), 103-104. doi:10.1177/003754977903200304
- Swift, K.M. (2009). *An Experimental Analysis of the Laminar Separation Bubble at Low Reynolds Numbers*. Master's Thesis, University of Tennessee.
- Tani, I. (1964). Low Speed Flows Involving Bubble Separations. *Progress in Aeronautical Science*, Vol. 5, 1964.
- Zhao, G., & Zhao, Q. (2014). Parametric analyses for synthetic jet control on separation and stall over rotor airfoil. *Chinese Journal of Aeronautics*, 27(5), 1051-1061. doi:10.1016/j.cja.2014.03.023
- Zhao, G., Zhao, Q., Gu, Y., & Chen, X. (2016). Experimental investigations for parametric effects of dual synthetic jets on delaying stall of a thick airfoil. *Chinese Journal of Aeronautics*, 29(2), 346-357. doi:10.1016/j.cja.2016.02.010
- Zhou, J., Zhong, S., & University of Manchester. (2010). *Numerical investigation of the behaviour of circular synthetic jets for effective flow separation control*. Manchester: University of Manchester.